

New 2-Pyrazoline and Hydrazone Derivatives as Potent and Selective Monoamine Oxidase A Inhibitors

Umut Salgin-Goksen, Gokcen Telli, Acelya Erikci, Ezgi Dedecengiz, Banu Cahide Tel, F. Betul Kaynak, Kemal Yelekcı, Gulberk Ucar,* and Nesrin Gokhan-Kelekci*

Cite This: *J. Med. Chem.* 2021, 64, 1989–2009

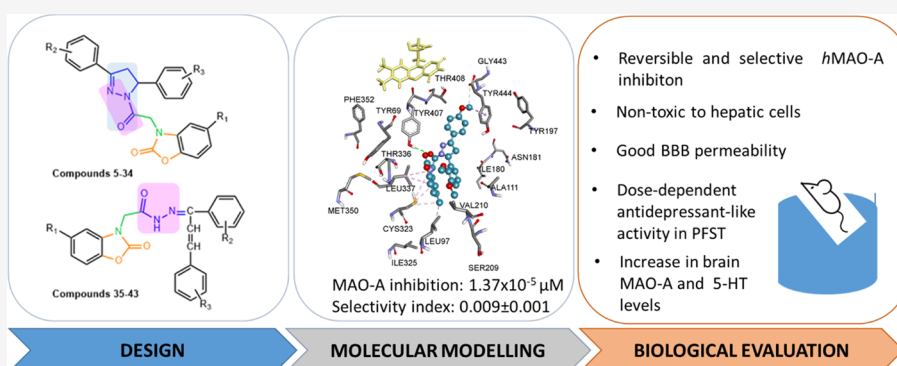
Read Online

ACCESS |

Metrics & More

Article Recommendations

Supporting Information



ABSTRACT: Thirty compounds having 1-[2-(5-substituted-2-benzoxazolinone-3-yl) acetyl]-3,5-disubstitutedphenyl-2-pyrazoline structure and nine compounds having *N'*-(1,3-disubstitutedphenylallylidene)-2-(5-substituted-2-benzoxazolinone-3-yl)-acetohydrazone skeleton were synthesized and evaluated as monoamine oxidase (MAO) inhibitors. All of the compounds exhibited selective MAO-A inhibitor activity in the nanomolar or low micromolar range. The results of the molecular docking for hydrazone derivatives supported the *in vitro* results. Five compounds, **6** ($0.008 \mu\text{M}$, Selectivity Index (SI): 9.70×10^{-4}), **7** ($0.009 \mu\text{M}$, SI: 4.55×10^{-5}), **14** ($0.001 \mu\text{M}$, SI: 8.00×10^{-4}), **21** ($0.009 \mu\text{M}$, SI: 1.37×10^{-5}), and **42** ($0.010 \mu\text{M}$, SI: 5.40×10^{-6}), exhibiting the highest inhibition and selectivity toward hMAO-A and nontoxic to hepatocytes were assessed for antidepressant activity as acute and subchronic in mice. All of these five compounds showed significant antidepressant activity with subchronic administration consistent with the increase in the brain serotonin levels and the compounds crossed the blood–brain barrier according to parallel artificial membrane permeation assay. Compounds **14**, **21**, and **42** exhibited an *ex vivo* MAO-A profile, which is highly consistent with the *in vitro* data.

INTRODUCTION

Depression is an important psychiatric disease and has a high incidence in the world. According to the World Health Organization, 350 million people are diagnosed with depression. It was predicted that between 2020 and 2030, depression will be the second important reason for disability in the world.¹ Depression can lead to the development of several second-order diseases besides the stress that is caused to the patients and their families.^{2–5} It was reported that anxiety disorders are observed before or during depression in 10–21% of children and adolescents.⁶

Monoamine oxidase inhibitors (MAOIs) were the first class of antidepressants to be developed. MAOIs are known for their mood-enhancing effect by virtue of blocking the breakdown of neurotransmitters by monoamine oxidase (MAO) (EC 1.4.3.4). Two isoforms of MAO have been discovered, which exhibit distinct interests to inhibitors and varying specificities to substrates.⁷ Adrenaline, noradrenalin, and serotonin are

metabolized mostly with MAO-A⁸ and β -phenylethylamine, and benzylamine is metabolized with MAO-B.⁹ Dopamine and some essential amines like tyramine interact with both isoforms of MAO.¹⁰ MAOIs are especially classified into two main categories in the clinic. The antidepressant activity is mostly associated with inhibition of MAO-A and the consequent ability to counter the decrement in brain noradrenaline (NE), dopamine (DA), and especially serotonin (5-HT) levels during the depression.² MAO-B inhibitors could be preferred in Alzheimer's and Parkinson's diseases.^{11,12} The use of MAOIs to treat major depressive disorders declined

Received: August 28, 2020

Published: February 3, 2021



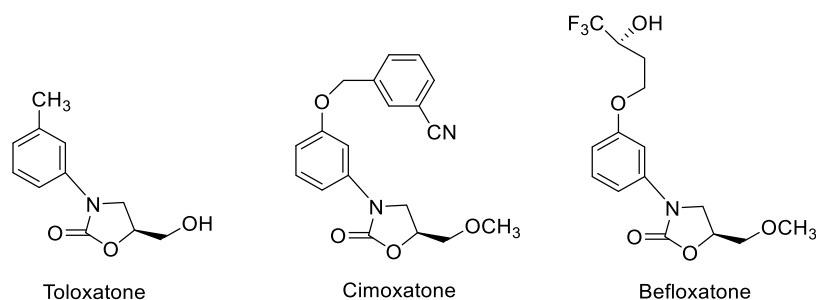


Figure 1. Aryloxazolidinone derivatives of MAOIs.

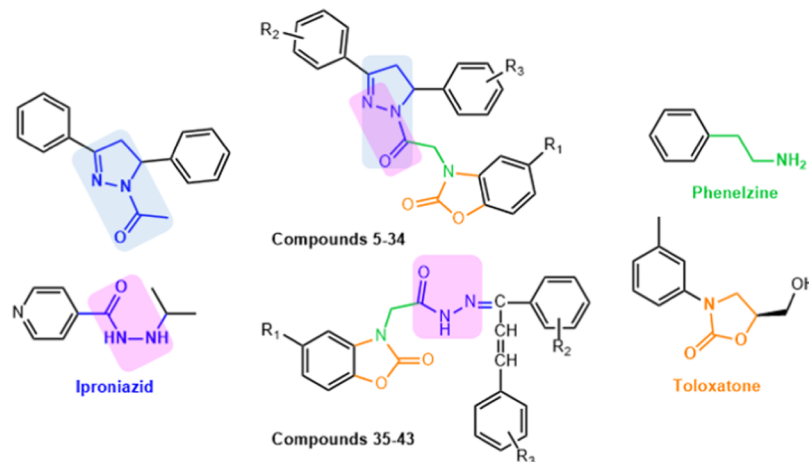


Figure 2. Overall design strategy for 2-pyrazoline and hydrazone derivatives (the color code indicates common chemical structures).

sharply after it was found that inhibition of MAO can lead to a severe cardiovascular event called the “cheese effect”, which is observed after intake of tyramine-containing foods. Studies focused on improving novel selective and reversible MAOIs with low tyramine potentiation properties.¹³

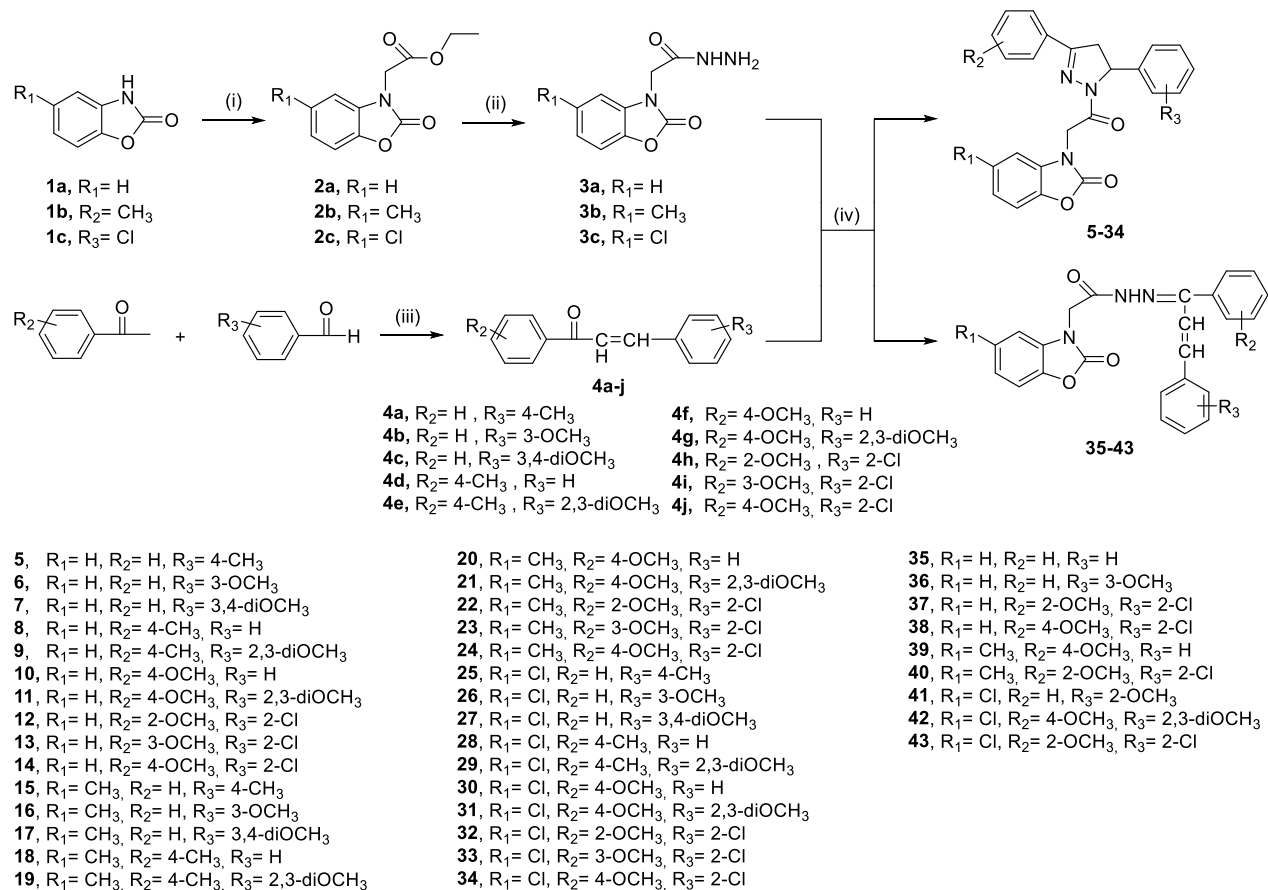
Since MAOIs can increase 5-HT, NE, and DA simultaneously in the brain, they have been considered for usage in treatment resistance depression instead of combination therapies such as combining an inhibitor of 5-HT-NE reuptake inhibitor with a certain dopaminergic drug or pairing a dopamine agonist with a selective serotonin reuptake inhibitor (SSRI) and a tricyclic antidepressants (TCA).³ The findings also indicate that these inhibitors have remarkable neuroprotective effects.⁴ The recently designed and synthesized highly selective and reversible MAOIs offer new opportunities for the development of superior antidepressant and anti-parkinsonian agents through the selective inhibition of MAO-A and MAO-B, respectively.

Classical MAOIs are analogues of natural MAO substrates and have a structure similar to that of phenylethylamines containing a reactive group, such as propargylamine and hydrazine, which allows the binding to the enzyme via covalent adducts resulting from bioactivation of the inhibitor to an electrophilic intermediate.¹⁴ 2-Pyrazoline derivatives are cyclic hydrazine moieties that are formed by the cyclization of linear hydrazine derivatives.¹⁵ Derivatives obtained by substitutions on the 2-pyrazoline nucleus preferably at the N1, C3, and C5 positions show a remarkable effect on the central nervous system (CNS).^{16–18} Chimenti et al. demonstrated that either the N1 acetyl group or N1-propanoyl substitution at position 1 increased potency and selectivity of these inhibitors.^{19–21}

Toloxatone (Humoryl) is the lead compound of aryloxazolidinones that are the relatively new classes of MAOIs (Figure 1). It is the first selective and reversible inhibitor of MAO-A and represented as an antidepressant to clinical use.²² Chemical modifications of tolaxatone generated more selective cimoxatone and befloxatone derivatives that are active at nanomolar concentrations.^{11,23}

According to the specified finding mentioned and the intent of developing new more selective and potent MAO-A inhibitors, we designed and synthesized some novel hybrid compounds bearing oxazolidinone and diazo cores (30 new 2-pyrazoline and 9 new hydrazone derivatives) as selective, potent MAO-A inhibitors with contribution of the docking studies (Figure 2 and Scheme 1). They were screened *in vitro* to determine their inhibitory actions on MAO isotypes. Since the biological activity of MAOIs depends heavily on their ability to cross the blood–brain barrier (BBB), the BBB permeability of selected new compounds was determined with the parallel artificial membrane permeation assay of BBB (PAMPA–BBB). Additionally, the potential acute and subchronic antidepressant activities of five compounds that exhibited the highest inhibitory selectivity and potency toward hMAO-A were determined. Since depression and its comorbid disorders are related to serotonin and dopamine interactions in the prefrontal cortex, the levels of 5-HT, DA, and 5-hydroxyindoleacetic acid (5-HIAA) and MAO activity were determined in brain tissues of experimental animals to evaluate the status of related neurotransmitters, their metabolites, and the MAO-metabolizing enzyme. Our data indicated that the compounds had an antidepressant-like activity in mice by the possible interaction with the serotonergic and monoaminergic systems.

Scheme 1. Synthesis and Structure of the Compounds



(i) ClCH₂COOC₂H₅, K₂CO₃, acetone; (ii) NH₂NH₂, ethanol; (iii) NaOH, water-ethanol, (iv) con.HCl, DMF, n-propanol

RESULTS AND DISCUSSION

Chemistry. A novel series of 1-[2-((5-methyl/chloro)-2-benzoxazolinone-3-yl)acetyl]-3,5-diaryl-2-pyrazoline **5–34** and *N'*-[(1,3-diaryl)allylidene]-2-[(5-methyl/chloro)-2-benzoxazolinone-3-yl]acetohydrazide **35–43** derivatives were synthesized according to the protocols summarized in [Scheme 1](#). The conditions of reactions and the characterization of compounds are explained in the [Experimental Section](#).

2-Benzoxazolinone **1a** and 5-methyl-2-benzoxazolinone **1b** were synthesized according to literature methods using 2-aminophenol/4-methyl-2-aminophenol and urea.²⁴ 5-Chloro-2-benzoxazolinone **1c** was commercially available. Ethyl ((5-methyl/chloro)-2-benzoxazolinone-3-yl) acetate derivatives **2a–2c**²⁵ were carried out by heating (5-methyl/chloro)-2-benzoxazolinone **1a–1c** with ethyl chloroacetate in K₂CO₃/acetone. The acid hydrazides **3a–3c** were prepared by nucleophilic substitution of **2a–2c** with hydrazine hydrate in ethanol.^{26–28} Treatment of appropriate aldehydes with acetophenone derivatives under basic conditions using the Claisen–Schmidt condensation²⁹ gave α,β -unsaturated carbonyl compounds (chalcones) **4a–4j**.

The reaction of hydrazides **3a–3c** with chalcones **4a–4j** in n-propanol under acidic condition yielded the corresponding 2-pyrazoline **5–34** and hydrazone derivatives **35–43** ([Scheme 1](#)). Due to the low stability of hydrazones and difficulties in their isolation, not all hydrazone compounds could be reached. The structures of the synthesized compounds were determined using IR, ¹H NMR, ¹³C NMR, and electrospray ionization

mass spectrometry (ESI-MS) techniques. The purity of compounds was determined by elemental analyses; the results were within $\pm 0.4\%$ of the theoretical values. Due to limited laboratory facilities, chiral separation of only one compound was made, the configurations of the separated enantiomers were determined by Vibrational Circular Dichroism, and their activities were examined.³⁰ The spectra of synthesized compounds are provided in the [Supporting Information](#).

X-ray Crystal Structure. The molecular structure of compounds **10** and **43** consists of two discrete entities. [Table S1](#) summarizes their main geometrical characteristics according to the numbering scheme ([Figures S1 and S2](#)). The most significant differences between these two compounds are the presence of a central pyrazoline ring in compound **10** and hydrazone moiety in compound **43** (The packing arrangements of both compounds are shown in [Figures S3 and S4](#)). In the crystal lattices of both compounds, there are multiple intermolecular interactions and strong intra- and intermolecular hydrogen bonds are responsible for the packing of the molecules ([Tables S2 and S3](#)).

Druglikeness and ADMET Predictions. Druglikeness of the designed compounds were predicted using AdmetSAR 2.0 server (<http://lmmd.ecust.edu.cn/admetSar1>)—a program that estimates the ADMET properties based on substructure pattern recognition and then uses a support vector machine algorithm to build a model.³¹ The chemical information of each designed compound was input in “smiles” format and the corresponding ADMET properties were estimated ([Table S4](#),

Table 1A. Experimental K_i Values of hMAO-Isoform Inhibition for Novel Newly Synthesized 2-Pyrazoline Derivatives and Reference Compounds^c

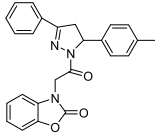
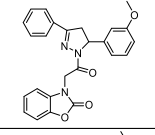
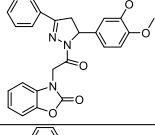
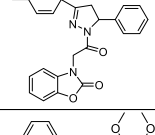
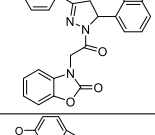
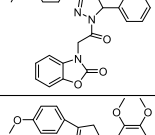
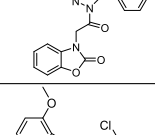
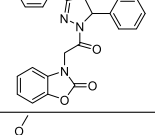
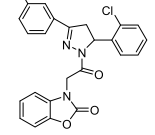
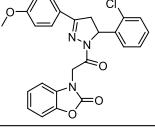
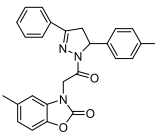
Compounds	Experimental K_i value for MAO-A (μM)**	Experimental K_i value for MAO-B (μM)**	Experimental SI^*	
5		0.004±0.001	8.95±0.53	4.46x10 ⁻⁴
6		0.008±0.001	8.25±0.19	9.70x10 ⁻⁴
7 ³⁰		0.009±0.001	20.00±1.55	4.55x10 ⁻⁵
8		0.019±0.005	5.55±0.16	0.003
9		0.028±0.001	120.50±8.25	2.32x10 ⁻⁴
10		0.011±0.001	9.00±0.34	0.001
11		0.125±0.001	255.00±19.50	4.90x10 ⁻⁴
12		0.013±0.001	1.15±0.09	0.011
13		0.060±0.003	7.50±0.37	0.008
14		0.001±10 ⁻⁴	1.25±0.060	8.00x10 ⁻⁴
15		0.008±0.001	5.22±0.21	0.002

Table 1A. continued

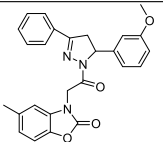
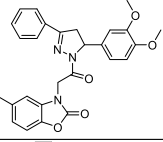
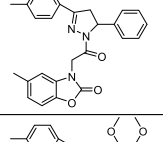
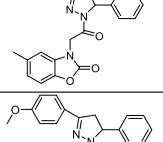
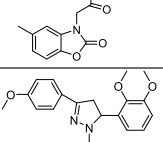
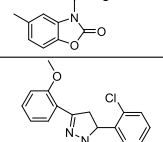
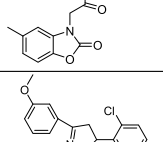
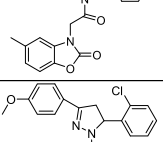
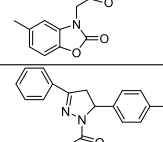
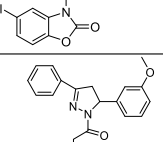
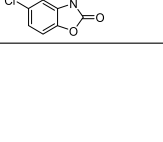
Compounds	Experimental K_i value for MAO-A (μM)**	Experimental K_i value for MAO-B (μM)**	Experimental S_i *	
16		0.005±0.001	21.30±1.16	2.35×10 ⁻⁴
17 ³⁴		0.170±0.01	41.3±2.55	0.004
18		0.050±0.002	29.00±1.05	0.002
19		0.266±0.001	52.00±1.99	0.005
20		0.800±0.05	7.50±0.33	0.107
21		0.009±0.001	655.20±32.70	1.37×10 ⁻⁵
22		0.308±0.02	15.90±1.11	0.019
23		0.011±0.001	24.33±1.54	4.52×10 ⁻⁴
24		0.018±0.003	0.40±0.002	0.045
25		0.040±0.002	8.55±0.49	0.005
26 ³⁵		0.985±0.062	1.00±0.05	0.985

Table 1A. continued

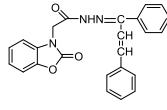
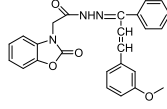
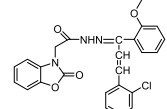
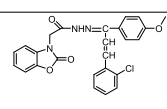
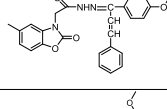
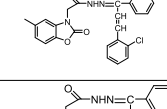
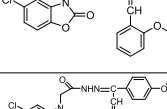
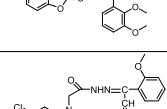
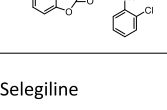
Compounds	Experimental K_i value for MAO-A (μM)**	Experimental K_i value for MAO-B (μM)**	Experimental SI*
27 ³⁵ 	3.000±0.213	50.16±2.88	0.06
28 	0.020±0.001	55.60±1.25	3.60x10 ⁻⁴
29 ³⁵ 	0.510±0.030	91.29±5.01	0.006
30 	0.004±0.001	1.95±0.11	0.002
31 	1.550±0.12	8000.00±436.00	1.94x10 ⁻⁴
32 	0.050±0.004	11.00±1.00	0.005
33 	0.120±0.009	2.55±0.16	0.05
34 	0.065±0.003	25.56±1.99	0.003
Selegiline	28.06±0.76	1.93±0.010	14.54
Lazabemide	>250.00	0.005±0.001	>10000
Moclobemide	0.10±0.001	7.66±0.006	0.013

*SI was calculated as $K_i(\text{MAO-A})/K_i(\text{MAO-B})$. ^bData demonstrate the mean \pm standard error of the mean (SEM) of three independent experiments. ^cMoclobemide and all synthesized compounds were found as reversible, competitive MAO-A inhibitors, while Selegiline (irreversible) and Lazabemide (reversible) were found as competitive MAO-B inhibitors.

Supporting Information). All designed compounds were found to be drug-like having obeyed Lipinski's "Rule of 5"³² and

Jorgensen's "Rule of 3".³³ All of the physicochemical parameters assessed were within the range of drug candidacy.

Table 1B. Calculated and Experimental K_i Values of hMAO-Isoform Inhibition for Novel Newly Synthesized Hydrazone Derivatives and Reference Compounds^c

Compounds	Calculated K_i values for MAOA/MAOB (μM)	Cal. SI ^a	Experimental K_i value for MAO-A/MAO-B (μM) ^{**}	Exp. SI ^a
35	 0.325x10 ³ / 24.23	1.34 x10 ⁻⁵	0.001±10 ⁻⁴ /19.00±1.38	5.26x10 ⁻⁵
36	 0.132x10 ³ / 6.56	2.01 x10 ⁻⁵	0.001±10 ⁻⁴ /8.90±0.99	1.12x10 ⁻⁴
37	 0.001 / 52.60	1.90 x10 ⁻⁵	0.004±10 ⁻⁴ /60.00±0.41	6.66x10 ⁻⁵
38	 0.394x10 ⁻³ / 23.69	1.66 x10 ⁻⁵	0.001±10 ⁻⁴ /35.00±2.80	3.43x10 ⁻⁵
39	 0.008 / 78.18	1.02 x10 ⁻⁴	0.012±0.001 /54.00±3.75	2.22x10 ⁻⁴
40	 0.001 / 19.01	5.26 x10 ⁻⁵	0.011±0.001 /16.55±1.80	6.65x10 ⁻⁴
41	 0.003x10 ⁻³ / 2.07	1.45 x10 ⁻⁶	0.001±10 ⁻⁴ /2.75±0.31	7.27x10 ⁻⁵
42	 0.004 / 9300.00	4.30 x10 ⁻⁷	0.010±0.01 /1850.00±89.50	5.40x10 ⁻⁶
43	 0.092x10 ⁻³ / 2.34	3.93 x10 ⁻⁵	0.001±10 ⁻⁴ /9.27±0.18	1.08x10 ⁻⁴
Selegiline	38.00 / 1.90	20.00	28.06±0.76 /1.93±0.010	14.54
Lazabemide	>250.00 / 0.65	>384.62	>250.00 /0.005±0.001	>10000
Moclobemide	0.13 / 17.21	0.008	0.10±0.001 /7.66±0.006	0.013

^aSI was calculated as $K_i(\text{MAO-A})/K_i(\text{MAO-B})$. ^bData demonstrate the mean \pm SEM of three independent experiments. ^cMoclobemide and all synthesized compounds were found as reversible, competitive MAO-A inhibitors, while Selegiline (irreversible) and Lazabemide (reversible) were found as competitive MAO-B inhibitors.

Evaluation of *In Vitro* Biological Screening Results and Molecular Modeling Data. hMAO activities were determined using Amplex Red MAO assay kit. The synthesized compounds were screened for their hMAO inhibitory activities using moclobemide (A-selective, reversible), selegiline (B-selective, irreversible), and lazabemide (B-selective, reversible) as reference inhibitors (Tables 1A and 1B). Specific enzyme

activities were calculated as 0.175 ± 0.012 nmol/mg/min ($n = 3$) for hMAO-A and 0.135 ± 0.009 nmol/mg/min ($n = 3$) for hMAO-B. Selectivity indexes (SI) were expressed as $K_i(\text{MAO-A})/K_i(\text{MAO-B})$.

Docking calculations were performed using AutoDock to determine binding affinities of the synthesized hydrazone derivatives (compounds 35–43) with MAO-A and MAO-B.

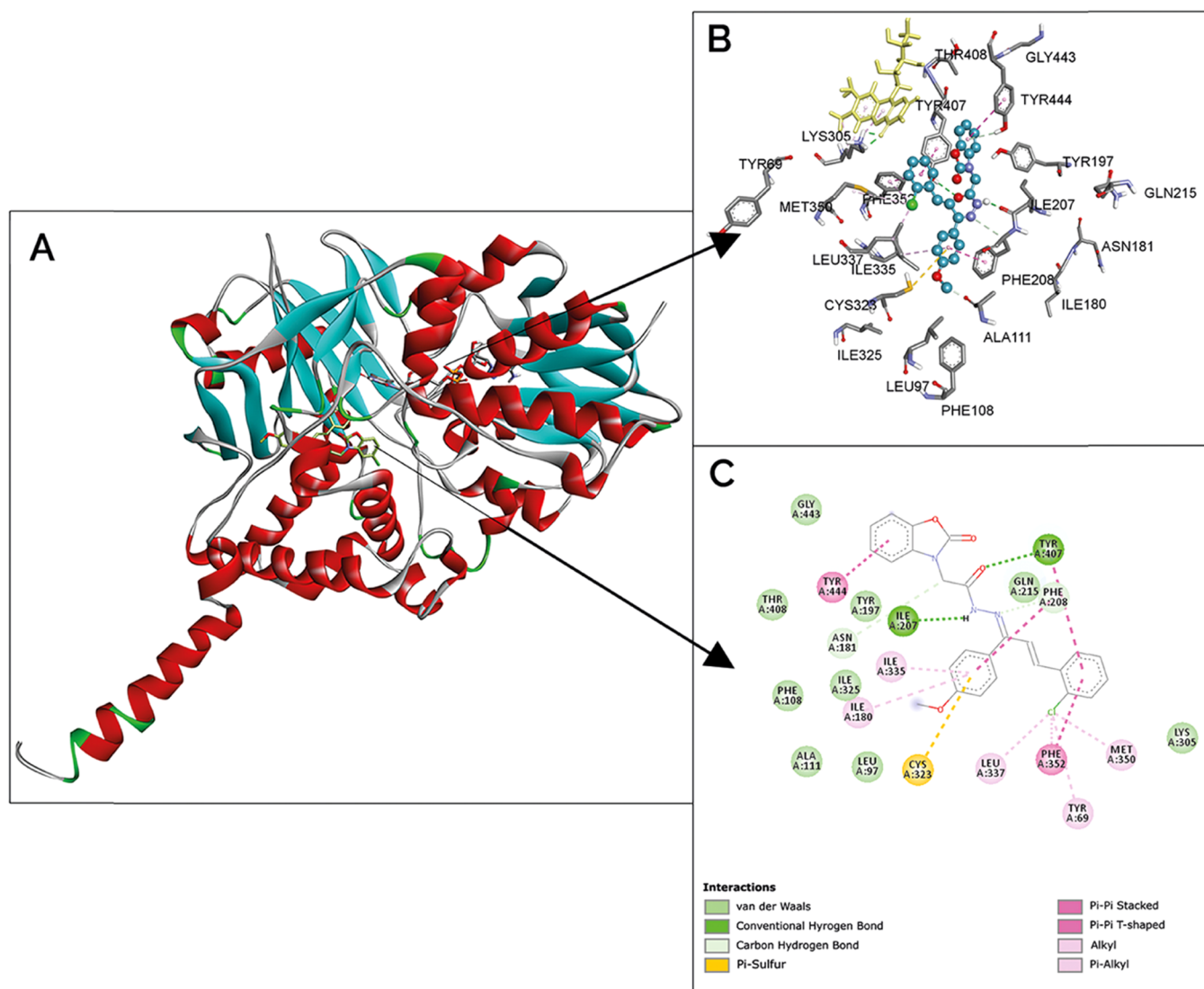


Figure 3. (A–C) 3D representations of compound **38** docked in the MAO-A (2Z5X) (A) active site. Magnified view of the active site (B). 2D interaction diagrams of compound **38** with amino acid residues lining the MAO-A active site (C).

Accelrys' (Biovia) Discovery Studio Protocols and visualization programs were used to render the poses of docked inhibitors in the active site of MAO-A and MAO-B isozymes. However, the computational inhibition constants obtained for each enantiomer of compounds **5–34** were not compared with the experimental inhibition constant measurements which were obtained for racemic forms. Thus, a correlation analysis would be insignificant for these compounds in the present study. All two-dimensional (2D) and three-dimensional (3D) pictures were produced using Biovia 4.6 visualization program. Two effective and selective compounds from hydrazone (**38** and **42**) group interacting with MAO-A and MAO-B were chosen.

Most of the newly synthesized pyrazolines (compounds **5–34**) and hydrazones (compounds **35–43**) inhibited hMAO-A potently and selectively. Among pyrazoline derivatives, compound **14** having 4-methoxy group at R_2 and 2-chlorine at R_3 exhibited the highest inhibitory activity toward hMAO-A with a K_i value of $0.001 \mu\text{M}$. This compound was more potent than moclobemide, the known selective and reversible MAO-A inhibitor inhibiting hMAO-A with the K_i value of $0.010 \pm 0.001 \mu\text{M}$.

Experimental data showed that the compound **21**, bearing 4-methoxy group at R_2 and 2,3-dimethoxy groups at R_3 inhibited hMAO-A potently with a K_i value of $0.009 \mu\text{M}$ (Table 1A).

In vitro screening data demonstrating that hydrazone derivative compounds **35**, **36**, **38**, **41**, and **43** showed the most inhibitory potency toward hMAO-A with the same K_i value of $0.001 \mu\text{M}$ indicated that the hMAO-A inhibitory ability of newly synthesized hydrazones is remarkably better than that of moclobemide ($K_i = 0.10 \mu\text{M}$) (Table 1B).

Molecular modeling studies of compound **38**, which is a hydrazone derivative of pyrazoline derivative, and compound **14** were also carried out for MAO-A and MAO-B isozymes (Figures 3 and 4). Figure 3A shows the orientation of compound **38** in the active site of MAO-A ($K_i = 0.394 \times 10^{-3} \mu\text{M}$). The benzoxazolinone ring of the inhibitor is inserted between TYR407 and TYR444 making a π - π stacked interaction with TYR444 (Figure 3B). Another hydrogen bond forms between the carbonyl groups of the inhibitor and TYR407. PHE352 forms a strong π - π interaction with the chlorophenyl ring of the inhibitor. CYS323 residue forms a π -sulfur interaction with the same ring. A hydrogen bond is formed between the NH moiety of the inhibitor and ILE207

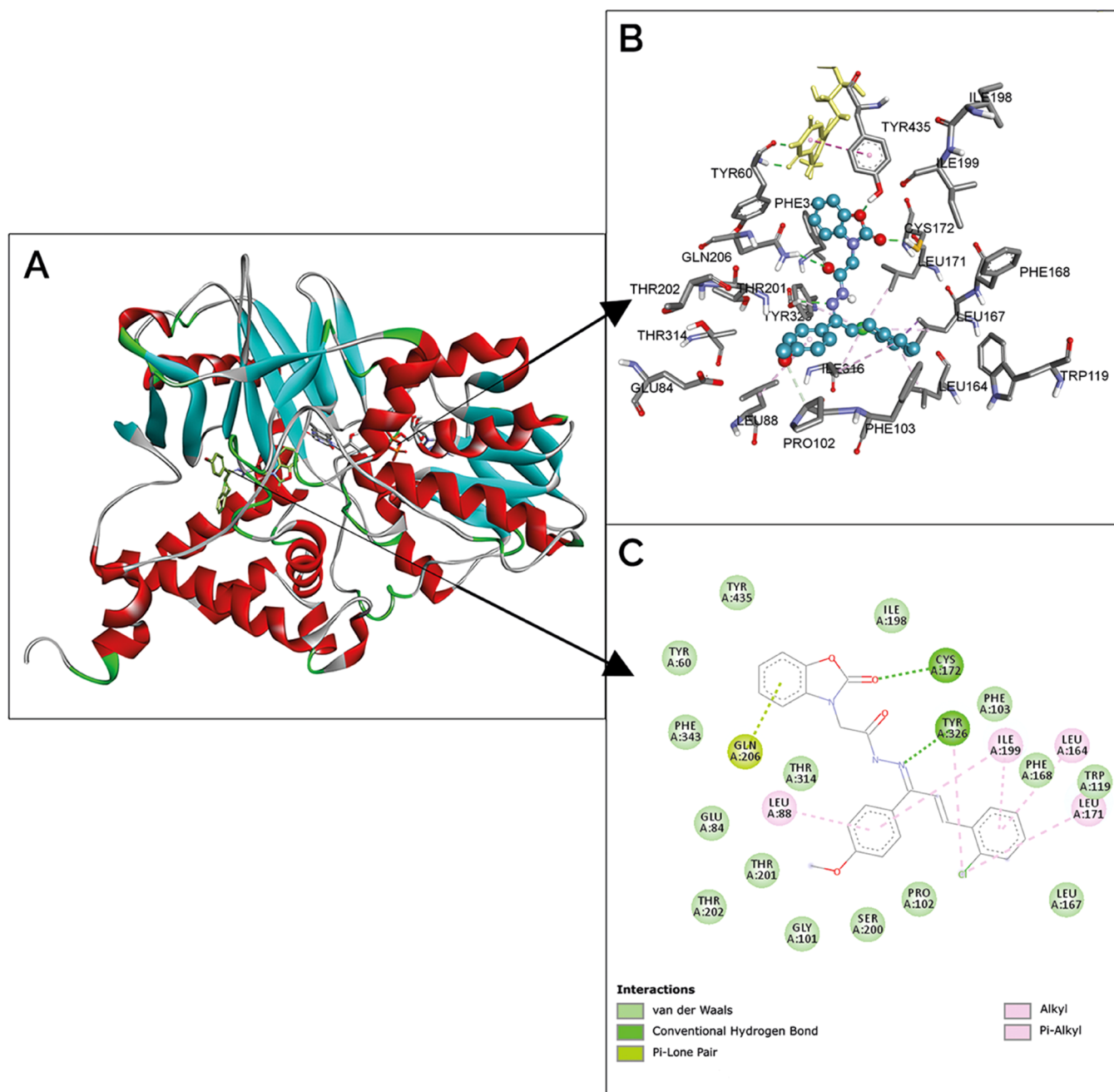


Figure 4. (A–C) 3D representations of compound **38** docked in the MAO-B (2V5Z) (B) active site. Magnified view of the active site (B). 2D interaction diagrams of compound **38** with amino acid residues lining the MAO-B active site (C).

backbone carbonyl group. In addition to these effective interactions, various hydrophobic and van der Waals interactions contribute to generating a better MAO-A inhibitor compared to MAO-B isozyme (Figure 3C).

Figure 4A shows compound **38** in the active site of MAO-B. The benzoxazolinone ring of the inhibitor is oriented away from the hydrophobic cage, making only one π -lone pair interaction with GLN206 (Figure 4B). The carbonyl group of the benzoxazolinone ring and double-bonded nitrogen atom of the inhibitor make two hydrogen bonds with CYS172 and TYR326, respectively. Various hydrophobic and van der Waals interactions occur between compound **38** and the active-site residues of MAO-B ($K_i = 23.69 \mu\text{M}$) (Figure 4C).

Among the hydrazones, compound **42** appeared the most selective hMAO-A inhibitor with an SI value of 5.40×10^{-6} (calculated SI: 4.30×10^{-7}). The selectivity of compound **42** toward hMAO-A isoform ($K_i = 0.010 \mu\text{M}$) was much higher than that of moclobemide (SI = 0.013) (Table 1B). According to the docking data, the benzoxazolinone ring of compound **42** was sandwiched between the TYR444 and TYR407 residues in the active site of hMAO-A making two strong π - π interactions with these residues while hMAO-B has only one π - π interaction between phenyl and TYR435, making compound **42** more potent hMAO-A inhibitor ($K_i = 0.004 \mu\text{M}$) than that of hMAO-B ($K_i = 9300.00 \mu\text{M}$) (Figure S5).

As a result, we found a good correlation between the experimental and calculated data for the hydrazones since

Table 2. Reversibility of hMAO Inhibition by the Selected Novel Derivatives^a

test compounds incubated with hMAO	hMAO-A activity before dialysis (%)	hMAO-A activity after dialysis (%)	hMAO-B activity before dialysis (%)	hMAO-B activity after dialysis (%)	reversibility
with no inhibitor	100 ± 0.00	100 ± 0.00	100 ± 0.00	100 ± 0.00	
selegiline	89.96 ± 2.25	90.01 ± 2.00	51.80 ± 2.30	52.40 ± 2.03	irreversible
lazabemide	11.00 ± 0.01	97.00 ± 1.16	89.00 ± 1.05	99.00 ± 1.70	reversible
moclobemide	36.00 ± 1.19	93.77 ± 2.16	88.00 ± 1.53	89.55 ± 1.90	reversible
6	24.55 ± 1.09	91.74 ± 1.93	85.00 ± 1.61	92.25 ± 1.66	reversible
7	23.11 ± 2.47	94.00 ± 3.21	78.90 ± 1.35	94.80 ± 2.07	reversible
14	18.11 ± 1.05	90.16 ± 1.88	78.20 ± 1.60	91.50 ± 2.64	reversible
21	22.16 ± 1.00	92.55 ± 1.39	74.19 ± 3.00	94.16 ± 3.71	reversible
41	19.55 ± 1.84	92.24 ± 2.60	77.29 ± 2.90	97.00 ± 2.33	reversible
42	20.16 ± 1.06	93.57 ± 2.46	82.37 ± 2.31	95.21 ± 3.27	reversible
43	21.91 ± 2.09	93.26 ± 3.00	77.22 ± 1.64	93.41 ± 2.11	reversible

^aData demonstrate mean ± SEM ($n = 3$).

Table 3. *In Vitro* Cytotoxicity of the Selected Novel Derivatives^{a,b}

compounds	viability (%)		
	7.5 μM	15 μM	30 μM
selegiline	90.00 ± 3.55	87.23 ± 2.90	84.00 ± 2.70
lazabemide	92.40 ± 2.00	89.66 ± 3.00	85.60 ± 2.76
moclobemide	90.80 ± 2.87	88.50 ± 2.90	86.00 ± 2.39
6	96.25 ± 2.05	88.29 ± 1.00	77.33 ± 1.97*
7	90.39 ± 3.00	88.25 ± 1.13	85.27 ± 3.37
14	91.23 ± 4.54	89.97 ± 2.03	85.00 ± 1.16
21	100.80 ± 5.60	99.60 ± 4.00	84.93 ± 8.59
41	91.35 ± 4.17	89.00 ± 2.66	87.67 ± 1.61
42	118.30 ± 4.50	99.12 ± 4.55	88.55 ± 2.39
43	92.11 ± 3.36	90.61 ± 3.73	87.40 ± 1.35

^aData demonstrate mean ± SEM ($n = 3$). ^bThe viability of cell was calculated as a percentage of the control. * $p < 0.05$ vs control.

these compounds do not have stereoisomers, and the correlation between the calculated and experimental data for these compounds can be successfully demonstrated.

Reversibility. The reversibility tests were performed for the most potent and selective hMAO-A inhibitors in this series (compounds 6, 7, 14, 21, 41, 42, and 43) using the dialysis method (Table 2). The compounds are found to be reversible hMAO inhibitors that have remarkable advantages compared to irreversible inhibitors with important side effects.

Cytotoxicity. The cytotoxicities of the most potent and selective compounds (compounds 6, 7, 14, 21, 41, 42, and 43) were tested in HepG2 cells at three concentrations (7.5, 15, and 30 μM). Data indicated that the selected compounds, except compound 6, which was slightly toxic to the cells at a concentration of 30 μM and at the title concentrations, were not toxic to hepatic cells (Table 3).

BBB Permeation. Since neuroactive drugs are required to cross the BBB to function,³⁶ PAMPA–BBB was performed to assess the capability of newly synthesized derivatives to cross the BBB. The assay was validated by comparing the permeabilities of nine commercial drugs with presented values (Table 4). A linear correlation was obtained with a plot of experimental vs bibliographic data ($R^2 = 0.9934$). According to the limits evaluated by Di et al.,³⁷ the novel compounds were classified as follows: $Pe (10^{-6} \text{ cm s}^{-1}) > 4.00$: CNS+ (high BBB permeation anticipated)

$Pe (10^{-6} \text{ cm s}^{-1}) < 2.00$: CNS– (low BBB permeation anticipated)

$Pe (10^{-6} \text{ cm s}^{-1})$ from 4.00 to 2.00: CNS ± (uncertain BBB permeation)

Table 4. Permeability of the Commercial Drugs Utilized for Assay Validation and of the Selected Novel Derivatives Determined Using the PAMPA–BBB Assay

compounds ^a	permeability ($10^{-6} \text{ cm s}^{-1}$) ^c		
	bibliography ^b	experimental	prediction
testosterone	17.0	16.00 ± 1.54	CNS+
verapamil	16.0	15.03 ± 1.23	CNS+
β-estradiol	12.0	9.99 ± 0.67	CNS+
progesterone	9.3	7.55 ± 0.56	CNS+
corticosterone	5.1	4.11 ± 0.35	CNS+
piroxicam	2.5	2.20 ± 0.11	CNS+/-
hydrocortisone	1.8	1.58 ± 0.12	CNS–
lomefloxacin	1.1	0.99 ± 0.06	CNS–
dopamine	0.2	0.32 ± 0.02	CNS–
6		8.90 ± 0.76	CNS+
7		9.44 ± 1.04	CNS+
14		11.00 ± 0.97	CNS+
21		8.05 ± 0.78	CNS+
41		14.55 ± 1.10	CNS+
42		15.60 ± 1.34	CNS+
43		14.02 ± 1.35	CNS+

^aDimethylsulfoxide (DMSO, 1% w/v) at 5 mg/mL was used to dissolve the compounds. They are diluted with PBS/EtOH (70:30). The compounds reached a 50 μg/mL final concentration. ^bBibliography is from ref 37. ^cData demonstrate mean ± SEM of three independent experiments.

Of the most selective and potent compounds exhibiting MAO-A activity, 6, 7, 14, 21, 41, 42, and 43 were included in

Table 5. Brain-Tissue MAO-A, 5-HT, DA, 5-HIAA, and 3,4-dihydroxyphenylacetic acid (DOPAC) Levels after the Acute and Subchronic Administrations of Test Compounds in Mice ($n = 6$)^a

compounds	MAO-A (nmol/min/mg)	5-HT ($\mu\text{g/g}$ tissue)	DA ($\mu\text{g/g}$ tissue)	5-HIAA ($\mu\text{g/g}$ tissue)	DOPAC ($\mu\text{g/g}$ tissue)
Acute Administration					
control	0.40 \pm 0.012	0.80 \pm 0.006	7.08 \pm 0.58	0.28 \pm 0.011	1.22 \pm 0.20
moclobemide	0.35 \pm 0.011**	0.83 \pm 0.012 *	7.10 \pm 0.09	0.32 \pm 0.012*	1.24 \pm 0.05
compound 6	0.31 \pm 0.007*** $\psi\psi\psi\psi$	0.88 \pm 0.011 *** $\psi\psi\psi$	7.08 \pm 0.21	0.32 \pm 0.009 *	1.23 \pm 0.27
compound 7	0.28 \pm 0.007*** $\psi\psi\psi\psi$	0.91 \pm 0.012 *** $\psi\psi\psi$	7.08 \pm 0.37	0.32 \pm 0.007*	1.23 \pm 0.10
compound 14	0.25 \pm 0.009*** $\psi\psi\psi\psi$	0.98 \pm 0.009 *** $\psi\psi\psi\psi$	7.10 \pm 0.42	0.35 \pm 0.009* $\psi\psi$	1.24 \pm 0.23
compound 21	0.23 \pm 0.014*** $\psi\psi\psi\psi$	1.10 \pm 0.026 *** $\psi\psi\psi\psi$	7.13 \pm 0.12	0.35 \pm 0.012*** $\psi\psi$	1.25 \pm 0.46
compound 42	0.20 \pm 0.014*** $\psi\psi\psi\psi$	1.24 \pm 0.114*** $\psi\psi\psi\psi$	7.16 \pm 0.38	0.45 \pm 0.011*** $\psi\psi\psi\psi$	1.25 \pm 0.24
Subchronic Administration					
control	0.40 \pm 0.005	0.78 \pm 0.01	7.45 \pm 0.22	0.18 \pm 0.01	1.54 \pm 0.12
moclobemide	0.33 \pm 0.014*	0.91 \pm 0.01 ***	7.40 \pm 0.12	0.23 \pm 0.01**	1.52 \pm 0.11
compound 6	0.29 \pm 0.005**	1.01 \pm 0.03*** ψ	7.30 \pm 0.42	0.24 \pm 0.05 *	1.59 \pm 0.11
compound 7	0.27 \pm 0.006*** $\psi\psi\psi$	1.04 \pm 0.04 *** ψ	7.31 \pm 0.55	0.24 \pm 0.01 **	1.58 \pm 0.08
compound 14	0.24 \pm 0.004*** $\psi\psi\psi\psi$	1.19 \pm 0.04 *** $\psi\psi\psi\psi$	7.28 \pm 0.65	0.31 \pm 0.01 *** $\psi\psi\psi$	1.57 \pm 0.11
compound 21	0.21 \pm 0.005*** $\psi\psi\psi\psi$	1.15 \pm 0.02 *** $\psi\psi\psi\psi$	7.43 \pm 0.51	0.30 \pm 0.01 *** $\psi\psi\psi\psi$	1.52 \pm 0.11
compound 42	0.16 \pm 0.009*** $\psi\psi\psi\psi$	1.28 \pm 0.01 *** $\psi\psi\psi\psi$	7.43 \pm 0.48	0.35 \pm 0.01*** $\psi\psi\psi\psi$	1.52 \pm 0.18

^a*** $p < 0.001$, ** $p < 0.01$, * $p < 0.05$ vs control; $\psi\psi\psi\psi$ $p < 0.001$, $\psi\psi\psi$ $p < 0.01$, ψ $p < 0.05$ vs moclobemide.

the assay. As seen in Table 5, they can successfully pass the BBB. Compounds 41, 42, and 43 exhibited the highest permeability considering that they may easily pass the BBB and achieve the targets in the CNS, which were in accordance with our design strategy. This result supports us to perform more detailed studies with these novel prodrugs.

Structure–Activity Relationship. The structure–activity relationships of the newly synthesized 2-pyrazoline derivatives were evaluated by considering the substitutions on the benzoxazolinone ring at the first position (R_1) and the phenyl rings at the third (R_2) and fifth positions (R_3). Although it is hard to make a definitive structure–activity relationship discussion, some generalizations could be postulated (Table 1A).

When compounds contain hydrogen, methyl, or chlorine at R_1 ; no substitution at R_2 ; and 4-methyl, 3-methoxy, or 3,4-dimethoxy substitutions at R_3 (compounds 5, 6, 7, 15, 16, 17, 25, 26, and 27) were compared, compounds 5, 6, and 7 with no substitution at R_1 appeared to be more potent than the ones with methyl or chlorine at R_1 . Compounds 15, 16, and 17, which have a methyl group at R_1 , inhibited hMAO-A more potently than those having a chlorine at R_1 (compounds 25, 26, and 27). Among the compounds with 4-methyl groups at R_3 (5, 15, and 25), the inhibitory potency of compounds 5 ($R_1 = \text{H}$) and 15 ($R_1: \text{CH}_3$) toward hMAO-A was found to be remarkably higher, about 10 times, than the inhibitory potency of compound 25, which has a chlorine at R_1 . Among the compounds carrying a 3-methoxy group at R_3 (compounds 6, 16, and 26), compound 6 with no substitution at R_1 and compound 16 with a methyl group at R_1 strongly inhibited hMAO-A, whereas the inhibitory potency of compound 26 with a chlorine at R_1 was relatively lower. Among the compounds with a 3,4-dimethoxy substitution at R_3 (compounds 7, 17, and 27), compound 7 with no substitution at R_1 and R_2 appeared as a potent hMAO-A inhibitor, whereas the inhibitory potency of compound 17 with a methyl at R_1 was found to be lower than that of compound 7. Compound 27 with a chlorine at R_1 showed the lowest inhibitory activity toward hMAO-A in this series.

In comparison to compounds with no substitution or 2,3-dimethoxy substitution at R_3 carrying 4-methyl substitution at

R_2 (compounds 8, 9, 18, 19, 28, and 29), the hMAO-A inhibitory potency of compounds with no substitution at R_3 (compounds 8, 18, and 28) was higher than those having a 2,3-dimethoxy substitution at R_3 (compounds 9, 19, and 29). Compounds 8 and 9 that have no substitution at R_1 showed more potent inhibitory activity toward hMAO-A than the others in this group.

When compounds carrying 4-methoxy at R_2 and having no substitution or having 2,3-dimethoxy or 2-chlorine substitutions at R_3 (compounds 10, 11, 14, 20, 21, 24, 30, 31, and 34) were compared, it was found that the compounds having 2,3-dimethoxy at R_3 (compounds 11, 21, and 31) possessed lower inhibitory activity toward hMAO-A than the other compounds in this group. Among the compounds having 2,3-dimethoxy at R_3 (compounds 11, 21, and 31), compound 21 which is bearing methyl at R_1 appeared as the most potent hMAO-A inhibitor. Among the compounds having no substitution at R_3 (compounds 10, 20, and 30), compound 30, which carries chlorine at R_1 , appeared as the most potent hMAO-A inhibitor. Among the compounds having 2-chlorine at R_3 (compounds 14, 24, and 34), compound 14, which has no substitution at R_1 , appeared as the most potent hMAO-A inhibitor. Compound 14 was found to be the most potent hMAO-A inhibitor in the novel 2-pyrazolines presented here.

When compounds having 2-chlorine at R_3 and 2-methoxy or 3-methoxy or 4-methoxy at R_2 (compounds 12, 13, 14, 22, 23, 24, 32, 33, and 34) were compared, compounds with no substitution at R_1 (compounds 12, 13, and 14) were found to inhibit hMAO-A more potently than the others. Compounds carrying 4-methoxy at R_2 (compounds 14, 24, and 34) inhibited hMAO-A more potently.

When compounds carrying no substitution at R_3 and having 4-methyl or 4-methoxy substitutions at R_2 (compounds 8, 10, 18, 20, 28, and 30) were compared, it was noted that compounds 8 and 10 that have no substitution at R_1 inhibited hMAO-A more potently than the others. Compounds 28 and 30 with chlorine at R_1 showed better inhibitory potency toward hMAO-A compared to those carrying methyl at R_1 .

Hydrazones having 2-methoxy at R_2 and 2-chlorine at R_3 (compounds 37, 40, and 43) were also evaluated. Compounds 37 with no substitution and compound 43 with chlorine

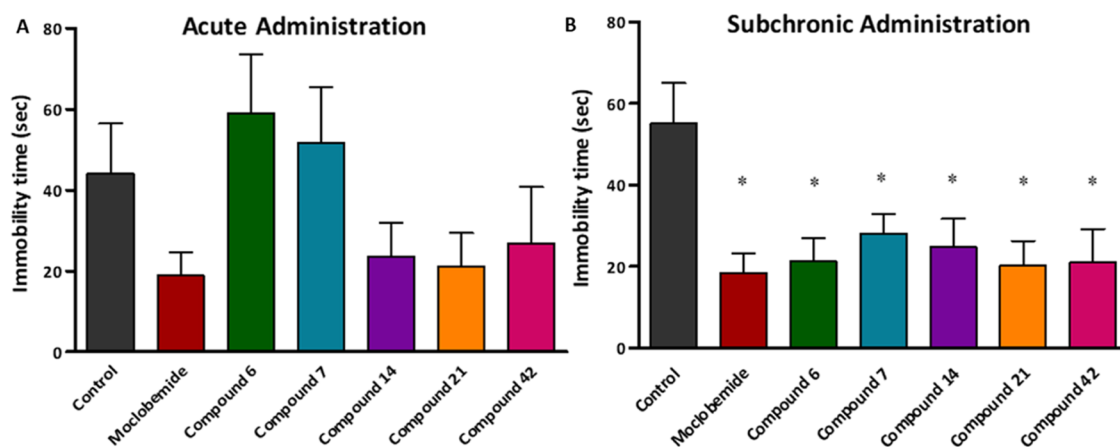


Figure 5. (A, B). Effects of a single-dose (A) and subchronic administrations (B) of the compounds and moclobemide on the immobility time in the PFST; $n = 8-12$, $*p < 0.05$. The immobility times of mice administrated with moclobemide or the test compounds were compared with the control.

Table 6. Dose–Response Study: Brain-Tissue MAO-A Activity; 5-HT, DA, 5-HIAA, and DOPAC Levels after the Subchronic Administration of Test Compounds 21 and 42 and Moclobemide in Mice ($n = 6$)^a

compounds	dose (mg/kg)	MAO-A (nmol/min/mg)	5-HT ($\mu\text{g/g}$ tissue)	DA ($\mu\text{g/g}$ tissue)	5-HIAA ($\mu\text{g/g}$ tissue)	DOPAC ($\mu\text{g/g}$ tissue)
control		0.39 ± 0.04	0.78 ± 0.01	7.45 ± 0.22	0.33 ± 0.02	1.54 ± 0.12
moclobemide	1	0.41 ± 0.05	0.78 ± 0.004	7.48 ± 0.06	0.33 ± 0.04	1.54 ± 0.05
	3	0.41 ± 0.05	0.79 ± 0.08	7.51 ± 0.14	0.32 ± 0.01	1.53 ± 0.05
	10	0.40 ± 0.06 *	0.82 ± 0.09 **	7.54 ± 0.05	0.30 ± 0.05	1.53 ± 0.07
	20	0.33 ± 0.01 **	0.91 ± 0.01 ***	7.58 ± 0.12	0.29 ± 0.01 **	1.53 ± 0.11
compound 21	1	0.39 ± 0.08 *** $\psi\psi\psi$	0.80 ± 0.05 ** $\psi\psi\psi$	7.35 ± 0.61	0.32 ± 0.04 ** ψ	1.46 ± 0.47
	3	0.34 ± 0.05 *** $\psi\psi\psi$	0.85 ± 0.05 *** $\psi\psi\psi$	7.44 ± 0.67	0.30 ± 0.03 *** $\psi\psi\psi$	1.53 ± 0.28
	10	0.27 ± 0.06 *** $\psi\psi\psi$	0.99 ± 0.05 *** $\psi\psi\psi$	7.44 ± 0.41	0.29 ± 0.01 ***	1.53 ± 0.11
	30	0.21 ± 0.04 *** $\psi\psi\psi$	1.10 ± 0.04 *** $\psi\psi\psi$	7.43 ± 0.51	0.22 ± 0.01 *** $\psi\psi\psi$	1.52 ± 0.11
compound 42	1	0.36 ± 0.03 *** $\psi\psi\psi$	0.81 ± 0.06 ** $\psi\psi\psi$	7.45 ± 1.00	0.32 ± 0.03 *	1.53 ± 0.47
	3	0.30 ± 0.05 *** $\psi\psi\psi$	0.83 ± 0.01 *** $\psi\psi$	7.44 ± 0.89	0.30 ± 0.05 ** $\psi\psi$	1.53 ± 0.24
	10	0.25 ± 0.07 *** $\psi\psi\psi$	0.92 ± 0.02 *** $\psi\psi\psi$	7.43 ± 0.65	0.26 ± 0.01 *** $\psi\psi\psi$	1.52 ± 0.30
	30	0.16 ± 0.09 *** $\psi\psi\psi$	1.19 ± 0.04 *** $\psi\psi\psi$	7.43 ± 0.48	0.18 ± 0.01 *** $\psi\psi\psi$	1.52 ± 0.18

^a*** $p < 0.001$, ** $p < 0.01$, * $p < 0.05$ vs control; $\psi\psi\psi$ $p < 0.001$, $\psi\psi$ $p < 0.01$, ψ $p < 0.05$ vs moclobemide.

substitution at R₁ were found to be more potent and selective inhibitors than compound 40 with a methyl group at R₁ (Table 1B).

Behavioral Evaluation. Porsolt's forced swim test (PFST) is based on behavioral despair, and it is a very commonly used method to evaluate antidepressant activity in drug development studies.^{38–40} An increase in the escape-directed behavior and the reduction of the immobility time indicate the antidepressant effect of tested compounds.^{41–43} The acute and subchronic antidepressant effects of selected compounds 6, 7, 14, 21, and 42 exhibiting the highest activity *in vitro* were assessed using PFST; moclobemide was used as the reference drug. To avoid the extra stress that may be caused by long-term oral gavage, 7-day subchronic application was preferred for the screening test. The *in vivo* oral dose of 30 mg/kg typically used in screening tests was used for testing the new compounds, while 20 mg/kg oral dose was used for moclobemide according to the previous data^{44,45} and the daily therapeutic dosage for a 70 kg adult human is 300–600 mg. Pharmacological analyses were performed 1 h after a single-dose (30 mg/kg) administration to evaluate the acute effects of the compounds and to observe the acute alterations in basal monoamine levels. Since the therapeutic response of antidepressant therapy generally begins in weeks, experiments

were also performed for 1 h after 7 days of subchronic administration of the compounds.^{46,47}

Acute, oral administration of compounds 14, 21, and 42 decreased the immobility time similar to the moclobemide. However, the decrease was not statistically significant compared to control. Compounds 6 and 7 did not reduce the immobility time compared to the control (Figure 5A). These data were from previous reports indicating that no behavioral changes are expected with a single-dose administration of antidepressants including moclobemide.⁴⁸ The immobility time was decreased after subchronic administration of compounds 6, 7, 14, 21, 42, and moclobemide (Figure 5B). No statistically significant differences were obtained between the groups.

The compounds 14, 21, and 42 and moclobemide decreased immobility time with acute administration, and the increasing antidepressant activity reached statistical significance after subchronic administration. On the other hand, compounds 6 and 7 did not provide any reduction in the immobility time with a single dose and caused an important decrease in immobility time with recurring doses. Therefore, it can be suggested that the pharmacokinetics of compounds 6 and 7 may be undergoing some problems such as first-pass effects that prevent their activity after a single-dose administration.

Following the behavioral assessments, the effects of acute and subchronic administrations of the compounds **6**, **7**, **14**, **21**, and **42** and moclobemide on the brain-tissue MAO-A selectivity were determined *ex vivo* by biochemical analysis. The MAO-A activity was reduced by both the acute and subchronic administrations of the test compounds in the brain (Table 5), suggesting that the compounds crossed the BBB. Subchronic administration of the new compounds and moclobemide caused more reduction in tissue MAO-A levels compared to acute administration. In agreement with the compounds' relatively higher inhibitory potency and better selectivity (Tables 1A and 1B), the compounds inhibited brain-tissue MAO-A activity more potently than that of moclobemide (Table 5). It is known that MAO catalyzes the deamination of biogenic amines including 5-HT and DA and produces 5-HIAA and DOPAC metabolites, respectively.¹³ 5-HT is more efficiently oxidized by MAO-A, while DA is a substrate for both subtypes. To examine the effect of the MAO-A inhibition on the brain levels of monoamines, brain-tissue levels of 5-HT, DA, and their main metabolites following the acute and subchronic administration of new compounds to mice were determined (Table 5). Brain-tissue 5-HT levels were significantly elevated, and 5-HIAA levels were reduced compared with those of the control group following both the acute and subchronic administrations of new compounds and moclobemide (Tables 5 and 6). It is known that the activity of MAO-A increases in depression and involves depletion of 5-HT in the brain; inhibition of MAO-A activity prevents the breakdown of 5-HT and increases 5-HT level in the synaptic cleft.¹³ On the other hand, the brain DA level was not affected by treatment with the new compounds and moclobemide. It was postulated that inhibition of MAO caused increased only in 5-HT concentrations and did not alter the DA level.

Our overall data demonstrate that new compounds strongly and selectively inhibit MAO-A and produce an antidepressant-like effect in mice possibly due to the increase in 5-HT brain levels caused by MAO-A inhibition. Although the compounds increased 5-HT levels in *ex vivo* analysis more than that of moclobemide, no difference was found in the antidepressant activity between the compounds and moclobemide. It can be thought that a 7-day subchronic treatment is not long enough for the compounds to show these marked changes in behavior.

It was previously postulated that MAO-inhibitor treatments can alter the motor functions,⁴⁹ which may affect the reliability of the PFST. Motor activity was assessed by open-field test (OFT) to eliminate any possible changes in the motor function. The distance moved in the box was measured following the administration to assess the locomotor activity. The new compounds and moclobemide caused no alteration in locomotor activity of mice (Figure 6).

Together with biochemical data, these findings indicate that the brain-tissue DA and DOPAC levels did not change following the administration of the new compounds, suggesting that the compounds did not have any significant side effects on the motor functions.

We also performed dose–response studies with the two most efficient compounds to investigate minimum effective doses of compounds **21** (a 2-pyrazoline derivative) and **42** (a hydrazone derivative) in mice. These compounds and moclobemide were administered to mice at 1, 3, 10, and 30 mg/kg doses for 7 days of subchronic oral administration. In PFST, moclobemide decreased the immobility time at 10 mg/kg dose compared with the control group, while compounds

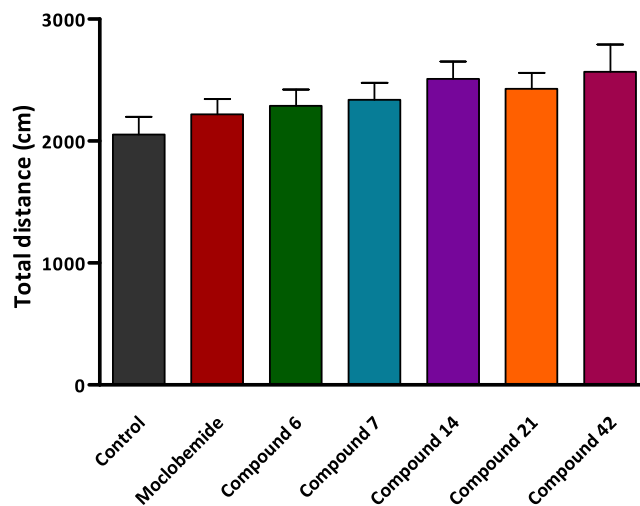


Figure 6. Total distance traveled in the open-field test by mice administrated subchronically 30 mg/kg of the test compounds and 20 mg/kg moclobemide. $n = 8–10$.

21 and **42** started to decrease the immobility time only at the 30 mg/kg dose (Figure 7A). However, the dose–response curves indicate that moclobemide at 20 mg/kg dose reached E_{max} value (i.e., it reached its maximum antidepressant-like activity), while compounds **21** and **42** did not reach such a plateau or the maximum activity. Therefore, these compounds may provide better antidepressant activity than moclobemide at higher doses (Figure 7B).

CONCLUSIONS

Depression is a life-threatening and highly debilitating neuropsychiatric disease. Reduced activity of serotonin-related pathways plays a causal role in the pathophysiology of depression. MAOIs, particularly MAO-A inhibitors, are found efficient in atypical and treatment resistance depression, anxiety, and bipolar depression. However, MAOIs are rarely used as a consequence of safety and intolerability problems and dietary restrictions. Selective reversible inhibitors of MAO-A (RIMAs) were introduced in the 1980s. In clinics, moclobemide is the only RIMA available; therefore, new potent RIMAs with fewer side effects are needed.

We have designed, prepared, and tested a new series of MAO-A-selective inhibitors based on the 2-pyrazoline and hydrazone scaffold. All of the compounds showed high inhibition in the nanomolar concentration and selectivity; in particular, compounds **14**, **21**, and **42** showed important potency and selectivity compared to the reference drugs clorgyline and moclobemide. Examination of the structure of the compounds indicated that the hydrazone derivatives were more selective and potent inhibitors of the MAO-A enzyme than 2-pyrazolines. To better understand the mechanism of selectivity and interaction of the novel compound, molecular modeling studies were performed for providing rational guidance for the design of novel potential leads for drugs. The results of the molecular docking supported the *in vitro* results.

The *in vitro* findings were confirmed *in vivo* by the PFST and *ex vivo* by measuring the alterations in the brain levels of 5-HT, DA, and their metabolites (5-HIAA, DOPAC) in mice. After acute administration, all compounds decreased 5-HIAA levels with a concomitant increase in 5-HT levels. However, these

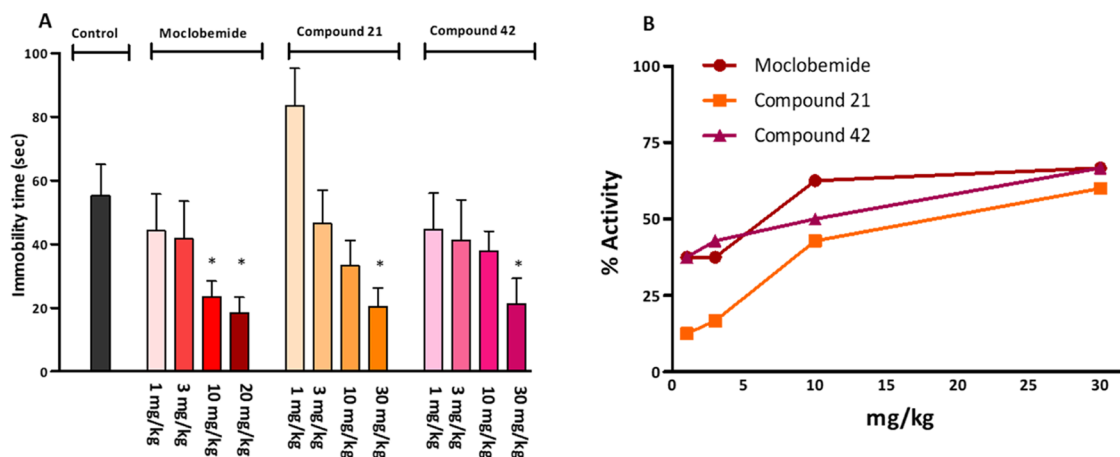


Figure 7. (A, B). Dose–response data with the PFST at 1, 3, 10, and 30 mg/kg doses of the test compounds and 1, 3, 10, and 20 mg/kg doses of moclobemide (A); $n = 8–12$, $*p < 0.05$. The immobility times of mice treated with test compounds or moclobemide were compared to those of the control mice. Dose–response curves of moclobemide and compounds 21 and 42. Increase in the activity % of the most effective compounds and moclobemide with increasing doses (B).

acute changes in brain monoamine levels were not reflected in behavior. On the other hand, all compounds exhibited statistically significant antidepressant activity after subchronic administration consistent with the increase in brain 5-HT and MAO-A levels. *Ex vivo* analysis showed that despite the high doses of test compounds being administered, the DA levels did not change compared to the control group, indicating a high MAO-A selectivity. Compounds 14, 21, and 42, the most potent and selective inhibitors of MAO-A, exhibited an *ex vivo* MAO-A profile, which is highly consistent with the *in vitro* data, indicating an increase in 5-HT and decrease in 5-HIAA brain levels.

It is not surprising that the compounds are less effective *in vivo* than *in vitro*, as antidepressants are generally known to show greater activity with prolonged administration. It was suggested that the 7-day subchronic treatment is not long enough to observe that apparent behavioral alterations in mice resulted from the depleted brain monoamine levels, and a longer administration time may be needed to provide higher antidepressant activity. It should also be noted that the compounds may undergo some physiological changes in the body due to their pharmacokinetic properties.

The dose–response curves (compounds 21 and 42) suggested that the efficacy of the compounds might be higher than that of moclobemide and that the compounds may show higher activity with increasing doses. However, the potency of the compounds was lower than that of moclobemide at lower doses.

The selected seven compounds showed no toxicity on hepatic cells. PAMPA–BBB showed that these compounds can cross the BBB, indicating that it might be possible to develop novel selective MAO-A inhibitors, based on this class of compounds, with a potential for generating improved treatment options for depression and mood disorders.

EXPERIMENTAL SECTION

Chemistry. All chemicals and solvents used in the chemical part were purchased from Merck A.G., Aldrich Chemical. Infrared (IR) spectra were ensured with a PerkinElmer SpectrumOne, Nicolet 520 FT-IR spectrometer, and the results were expressed in wavenumber (cm^{-1}). ^1H NMR spectra were recorded on a Bruker 400 MHz UltraShield spectrometer utilizing dimethylsulfoxide or acetone with chemical shifts being reported as δ (ppm) from tetramethylsilane

(TMS). ^{13}C NMR spectra were recorded on a Varian Mercury 400 MHz high-performance digital FT-NMR spectrometer utilizing dimethylsulfoxide or acetone with chemical shifts being reported as δ (ppm). Mass spectra were recorded using a Waters 2695 Alliance Micromass ZQ LC/MS spectrometer in methanol according to the ESI⁺ technique. Melting points were determined using a Thomas Hoover Capillary melting point apparatus and were uncorrected. Thin-layer chromatography (TLC) was performed using Merck 60 F254 silica gel plates (E. Merck, Darmstadt, Germany). The purity of the compounds was checked by elemental analyses (C, H, N) performed on a LECO CHNS 932 analyzer in the laboratory of the Ankara University. All compounds were obtained with a purity of >95%. ^1H NMR, ^{13}C NMR, and mass interpretations and all spectral data of the synthesized compounds are provided in the Supporting Information.

General Procedure for the Preparation of 1,3-Di(substituted)-phenyl-2-propen-1-ones (4) (Chalcones). Chalcone derivatives were synthesized by condensing acetophenone (10 mmol) and benzaldehyde (10 mmol) derivatives in the presence of sodium hydroxide (12.5 mmol) in water and ethanol (5/3 mL) at 0 °C for 1 h. The solid mass separated out was filtered, dried, and crystallized from methanol.²⁹ **4a:** m.p. 95–97 °C;⁵⁰ 95–96 °C (ethanol). **4b:** m.p. 62–63 °C;⁵¹ 61–62 °C (ethanol). **4c:** m.p. 86.5–88.5 °C;⁵² 90–92 °C. **4d:** m.p. 55–57 °C;⁵³ (57–58 °C). **4e:** This compound has been synthesized previously,^{54,55} but its spectral properties have not been elucidated. It is a yellow solid; yield 96% (2.699 g); mp 75.5–77.5 °C. IR cm^{-1} : 3007, 2933, 2838 (C–H), 1660 (C=O), 1609, 1574, 1475, 1428 (C=C), 1266, 1227, 1180, 1069 (C–O–C). ^1H NMR (DMSO- d_6 , 400 MHz) δ (ppm): 2.42 (s, 3H, $-\text{CH}_3$), 3.87 (s, 3H, $-\text{OCH}_3$), 3.88 (s, 3H, $-\text{OCH}_3$), 6.96 (dd, 1H, phenyl-H, J_1 :8.4 Hz, J_2 :1.2 Hz), 7.08 (t, 1H, phenyl-H), 7.25–7.26 (m, 1H, phenyl-H), 7.29 (d, 2H, 4-methylphenyl-2H, J : 8.0 Hz), 7.59 (d, 1H, $-\text{CO}-\text{CH}=\text{C}$, J : 15.6 Hz), 7.93 (d, 2H, 4-methylphenyl-2H, J : 8.0 Hz), 8.08 (d, 1H, phenyl- $\text{CH}=\text{C}$, J : 15.6 Hz). MS (ESI) m/z (%): 283 [$\text{M}+\text{H}$]⁺ (100%). Elemental analysis calculated (%) for $\text{C}_{18}\text{H}_{18}\text{O}_3$: C 76.57, H 6.43. Found: C 76.84, H 6.52. **4f:** m.p. 103–105 °C;⁵⁶ 103–105 °C (ethanol), **4g:** m.p. 102–103 °C;⁵⁷ 102–103 °C, **4h:** m.p. 56–58 °C;⁵⁸ 65–67 °C (methanol:water), **4i:** This compound has been synthesized previously,⁵⁹ but its spectral properties have not been elucidated. It is a yellow solid; yield 95% (2.581 g); m.p. 55–57 °C. IR cm^{-1} : 3070, 2938, 2837 (C–H), 1661 (C=O), 1589, 1466, 1430 (C=C), 1321, 1271, 1256, 1199, 1173, 1032 (C–O–C). ^1H NMR (DMSO- d_6 , 400 MHz) δ (ppm): 3.86 (s, 3H, $-\text{OCH}_3$), 7.26 (dd, 1H, phenyl-H, J_1 :8.0 Hz, J_2 :2.0 Hz), 7.44–7.49 (m, 2H, phenyl-2H), 7.52 (d, 1H, phenyl-H, J : 8.0 Hz), 7.58 (dd, 1H, phenyl-H, J_1 :7.6 Hz, J_2 :1.6 Hz), 7.63 (m, 1H, phenyl-H), 7.78 (d, 1H, phenyl-H, J : 7.6 Hz), 7.97 (d, 1H, $-\text{CO}-\text{CH}=\text{C}$, J : 16.0 Hz), 8.05 (d, 1H, phenyl- $\text{CH}=\text{C}$, J : 15.6

H_z), 8.24 (dd, 1H, phenyl-H, J₁:7.2 Hz, J₂:2.4 Hz). MS (ESI) *m/z* (%): 297 [M + Na + 2]⁺ (36%), 296 [M + H + Na]⁺, 295 [M + Na]⁺ (100%), 275 [M + H + 2]⁺ (16%), 273 [M + H]⁺ (49%), 237 [M⁺ - Cl]⁺, 167 [(2-Cl)C₆H₄-CH=CH-CO+2]⁺, 165 [(2-Cl)C₆H₄-CH=CH-CO]⁺, 135 [(3-CH₃O)C₆H₄-CO]⁺. Elemental analysis calculated (%) for C₁₆H₁₃ClO₂: C 70.46, H 4.80; Found: C 69.58, H 4.81. 4j: m.p 90–92 °C.⁶⁰ (*E* isomer 87.8–89.3 °C, methanol: dichloromethane).

General Procedure for the Preparation of 1-[2-(5-Substituted-2-benzoxazolinone-3-yl)acetyl]-3,5-di(substituted)phenyl-2-pyrazolines (5–34) and N'-[1,3-Di(substituted)phenylallylidene]-2-(5-substituted-2-benzoxazolinone-3-yl)acetohydrazide (35–43). 2-(5-Substituted-2-benzoxazolinone-3-yl)acetylhydrazine (3 mmol) was dissolved in 2 mL of *N,N*-dimethylformamide (DMF) and 20 mL of *n*-propanol. 1,3-Di(substituted)phenyl-2-propen-1-one (3 mmol) and eight drops of hydrochloric acid were added to this solution and refluxed for approximately 120 h. At the end of the reaction, pyrazoline, hydrazone, or a mixture of the two was obtained as the product. The reaction mixture was then cooled, and the solid precipitated was recrystallized. If solid was not precipitated or precipitated clearly, the solution was purified by column chromatography. Due to the low stability of hydrazones and difficulties in their isolation, not all hydrazone compounds could be reached.

1-[2-(2-Benzoxazolinone-3-yl)acetyl]-3-phenyl-5-(4-methylphenyl)-2-pyrazoline (5). White solid; mp 214.5–215.5 °C. IR cm⁻¹: 3059, 2921 (C–H), 1778, 1668 (C=O), 1601, 1487, 1440 (C=C, C=N), 1365, 1314, 1231, 1148, 1018 (C–O–C, C–N). For ¹H NMR, ¹³C NMR, and mass data, see the [Supporting Information](#). Elemental analysis calculated (%) for C₂₅H₂₁N₃O₄: C 72.98, H 5.14, N 10.21. Found: C 72.73, H 5.24, N 10.39.

1-[2-(2-Benzoxazolinone-3-yl)acetyl]-3-phenyl-5-(3-methoxyphenyl)-2-pyrazoline (6). White solid; mp 185.5–187 °C. IR cm⁻¹: 3067, 3037, 2844 (C–H), 1752, 1668 (C=O), 1596, 1490, 1433 (C=C, C=N), 1370, 1241, 1135, 1015 (C–O–C, C–N). For ¹H NMR, ¹³C NMR, and mass data, see the [Supporting Information](#). Elemental analysis calculated (%) for C₂₅H₂₁N₃O₄: C 70.25, H 4.95, N 9.83. Found: C 70.47, H 5.11, N 9.90.

1-[2-(2-Benzoxazolinone-3-yl)acetyl]-3-phenyl-5-(3,4-dimethoxyphenyl)-2-pyrazoline (7).³⁰ White solid; mp 204–204.5 °C. IR cm⁻¹: 3069, 3000, 2944, 2839 (C–H), 1769, 1680 (C=O), 1603, 1520, 1490, 1439 (C=C, C=N), 1369, 1237, 1140, 1020 (C–O–C, C–N). For ¹H NMR, ¹³C NMR, and mass data, see the [Supporting Information](#). Elemental analysis calculated (%) for C₂₄H₂₃N₃O₅: C 68.26, H 5.07, N 9.19. Found: C 68.18, H 5.06, N 9.15.

1-[2-(2-Benzoxazolinone-3-yl)acetyl]-3-(4-methylphenyl)-5-phenyl-2-pyrazoline (8). White solid; mp 200–201.5 °C. IR cm⁻¹: 3067, 3040 (C–H), 1769, 1659 (C=O), 1603, 1483, 1440 (C=C, C=N), 1366, 1244, 1100, 1018 (C–O–C, C–N). For ¹H NMR, ¹³C NMR, and mass data, see the [Supporting Information](#). Elemental analysis calculated (%) for C₂₅H₂₁N₃O₄: C 72.98, H 5.14, N 10.21. Found: C 72.74, H 4.97, N 10.26.

1-[2-(2-Benzoxazolinone-3-yl)acetyl]-3-(4-methylphenyl)-5-(2,3-dimethoxyphenyl)-2-pyrazoline(9). Cream solid; mp 181–183 °C. IR cm⁻¹: 2941, 2831 (C–H), 1762, 1673 (C=O), 1609, 1477, 1447 (C=C, C=N), 1367, 1300, 1271, 1078, 1022 (C–O–C, C–N). For ¹H NMR, ¹³C NMR, and mass data, see the [Supporting Information](#). Elemental analysis calculated (%) for C₂₇H₂₅N₃O₅: C 68.78, H 5.34, N 8.91. Found C 68.81, H 5.03, N 9.11.

1-[2-(2-Benzoxazolinone-3-yl)acetyl]-3-(4-methoxyphenyl)-5-phenyl-2-pyrazoline (10). Cream solid; mp 219–219.5 °C. IR cm⁻¹: 2957, 2835 (C–H), 1762, 1656 (C=O), 1606, 1518, 1494, 1453 (C=C, C=N), 1370, 1316, 1264, 1108, 1045, (C–O–C, C–N). For ¹H NMR, ¹³C NMR, and mass data, see the [Supporting Information](#). Elemental analysis calculated (%) for C₂₅H₂₁N₃O₄: C 70.25, H 4.95, N 9.83. Found: C 69.79, H 4.81, N 9.83.

1-[2-(2-Benzoxazolinone-3-yl)acetyl]-3-(4-methoxyphenyl)-5-(2,3-dimethoxyphenyl)-2-pyrazoline (11). Cream solid; mp 194–195 °C. IR cm⁻¹: 3011, 2928, 2838 (C–H), 1766, 1676 (C=O), 1603, 1477, 1454 (C=C, C=N), 1390, 1251, 1172, 1072, 1026 (C–O–C, C–N). For ¹H NMR, ¹³C NMR, and mass data, see the [Supporting Information](#). Elemental analysis calculated (%) for

C₂₇H₂₅N₃O₆: C 66.52, H 5.17, N 8.62. Found: C 66.47, H 5.47, N 8.38.

1-[2-(2-Benzoxazolinone-3-yl)acetyl]-3-(2-methoxyphenyl)-5-(2-chlorophenyl)-2-pyrazoline (12). Cream solid; mp 200–201 °C. IR cm⁻¹: 1759, 1670 (C=O), 1599, 1492 (C=C, C=N), 1374, 1253, 1121, 1032 (C–O–C, C–N). For ¹H NMR, ¹³C NMR, and mass data, see the [Supporting Information](#). Elemental analysis calculated (%) for C₂₅H₂₀ClN₃O₄: C 65.01, H 4.36, N 9.10. Found: C 64.75, H 4.31, N 9.02.

1-[2-(2-Benzoxazolinone-3-yl)acetyl]-3-(3-methoxyphenyl)-5-(2-chlorophenyl)-2-pyrazoline (13). White solid; mp 220.5–221.5 °C. IR cm⁻¹: 3060, 2931, 2835 (C–H), 1772, 1676 (C=O), 1560, 1463 (C=C, C=N), 1307, 1271, 1151, 1118, 1035 (C–O–C, C–N). For ¹H NMR, ¹³C NMR, and mass data, see the [Supporting Information](#). Elemental analysis calculated (%) for C₂₅H₂₀ClN₃O₄: C 65.01, H 4.36, N 9.10. Found: C 64.74, H 4.26, N 9.06.

1-[2-(2-Benzoxazolinone-3-yl)acetyl]-3-(4-methoxyphenyl)-5-(2-chlorophenyl)-2-pyrazoline (14). White solid; mp 237–238 °C. IR cm⁻¹: 3054, 2934, 2828 (C–H), 1759, 1666 (C=O), 1606, 1493, 1463 (C=C, C=N), 1398, 1248, 1175, 1039 (C–O–C, C–N). For ¹H NMR, ¹³C NMR, and mass data, see the [Supporting Information](#). Elemental analysis calculated (%) for C₂₅H₂₀ClN₃O₄: C 65.01, H 4.36, N 9.10. Found: C 65.16, H 4.37, N 9.22.

1-[2-(5-Methyl-2-benzoxazolinone-3-yl)acetyl]-3-phenyl-5-(4-methylphenyl)-2-pyrazoline (15). White solid; mp 185–186 °C. IR cm⁻¹: 2925 (C–H), 1768, 1677 (C=O), 1495, 1440 (C=C, C=N), 1387, 1238, 1114, 1018 (C–O–C, C–N). For ¹H NMR, ¹³C NMR, and mass data, see the [Supporting Information](#). Elemental analysis calculated (%) for C₂₆H₂₃N₃O₃: C 73.39, H 5.45, N 9.88. Found: C 73.20, H 5.18, N 9.81.

1-[2-(5-Methyl-2-benzoxazolinone-3-yl)acetyl]-3-phenyl-5-(3-methoxyphenyl)-2-pyrazoline (16). White-cream solid; mp 186–186.5 °C. IR cm⁻¹: 3055, 2933, 2830 (C–H), 1758, 1671 (C=O), 1601, 1499, 1440 (C=C, C=N), 1389, 1258, 1241, 1136, 1042, 1022 (C–O–C, C–N). For ¹H NMR, ¹³C NMR, and mass data, see the [Supporting Information](#). Elemental analysis calculated (%) for C₂₆H₂₃N₃O₄: C 70.74, H 5.25, N 9.52. Found: C 70.80, H 5.31, N 9.53.

1-[2-(5-Methyl-2-benzoxazolinone-3-yl)acetyl]-3-phenyl-5-(3,4-dimethoxyphenyl)-2-pyrazoline (17).³⁴ White solid; mp 175–176 °C. IR cm⁻¹: 3067, 2937, 2838 (C–H), 1767, 1672 (C=O), 1515, 1499, 1448 (C=C, C=N), 1392, 1235, 1137, 1027 (C–O–C, C–N). For ¹H NMR, ¹³C NMR, and mass data, see the [Supporting Information](#). Elemental analysis calculated (%) for C₂₇H₂₅N₃O₅: C 68.78, H 5.34, N 8.91. Found: C 68.40, H 5.31, N 8.84.

1-[2-(5-Methyl-2-benzoxazolinone-3-yl)acetyl]-3-(4-methylphenyl)-5-phenyl-2-pyrazoline (18). Cream solid; mp 203–204.5 °C. IR cm⁻¹: 3049, 3025, 2916 (C–H gerilim), 1756, 1675 (C=O), 1498, 1453 (C=C, C=N), 1393, 1240, 1135, 1026 (C–O–C, C–N). For ¹H NMR, ¹³C NMR, and mass data, see the [Supporting Information](#). Elemental analysis calculated (%) for C₂₆H₂₃N₃O₃: C 73.39, H 5.45, N 9.88. Found: C 72.98, H 5.69, N 9.81.

1-[2-(5-Methyl-2-benzoxazolinone-3-yl)acetyl]-3-(4-methylphenyl)-5-(2,3-dimethoxyphenyl)-2-pyrazoline (19). Cream solid; mp 191.5–192.5 °C. IR cm⁻¹: 2944, 2838 (C–H), 1778, 1672 (C=O), 1487, 1444 (C=C, C=N), 1377, 1266, 1085 (C–O–C, C–N). For ¹H NMR, ¹³C NMR, and mass data, see the [Supporting Information](#). Elemental analysis calculated (%) for C₂₈H₂₇N₃O₅: C 69.26, H 5.60, N 8.65. Found: 69.30, H 5.56, N 8.73.

1-[2-(5-Methyl-2-benzoxazolinone-3-yl)acetyl]-3-(4-methoxyphenyl)-5-phenyl-2-pyrazoline (20). Cream solid; mp 188–189.5 °C. IR cm⁻¹: 1755, 1672 (C=O), 1605, 1452 (C=C, C=N), 1392, 1262, 1172, 1026 (C–O–C, C–N). For ¹H NMR, ¹³C NMR, and mass data, see the [Supporting Information](#). Elemental analysis calculated (%) for C₂₆H₂₃N₃O₄: C 70.74, H 5.25, N 9.52. Found: C 70.32, H 5.43, N 9.51.

1-[2-(5-Methyl-2-benzoxazolinone-3-yl)acetyl]-3-(4-methoxyphenyl)-5-(2,3-dimethoxyphenyl)-2-pyrazoline (21). White solid; mp 211–212.5 °C. IR cm⁻¹: 2941, 2834 (C–H), 1759, 1672 (C=O), 1605, 1495, 1444 (C=C, C=N), 1392, 1310, 1243, 1176, 1081 (C–O–C, C–N). For ¹H NMR, ¹³C NMR, and mass data, see the

Supporting Information. Elemental analysis calculated (%) for $C_{28}H_{27}N_3O_6$: C 67.06, H 5.43, N 8.38. Found: C 67.15, H 5.71, N 8.38.

1-[2-(5-Methyl-2-benzoxazolinone-3-yl)acetyl]-3-(2-methoxyphenyl)-5-(2-chlorophenyl)-2-pyrazoline (22). Cream solid; mp 200–202 °C. IR cm^{-1} : 1767, 1668 (C=O), 1605, 1471, 1450 (C=C, C=N), 1393, 1240, 1027 (C–O–C, C–N). For 1H NMR, ^{13}C NMR, and mass data, see the [Supporting Information](#). Elemental analysis calculated (%) for $C_{26}H_{22}ClN_3O_4$: C 65.62, H 4.66, N 8.83. Found: C 65.21, H 4.68, N 8.97.

1-[2-(5-Methyl-2-benzoxazolinone-3-yl)acetyl]-3-(3-methoxyphenyl)-5-(2-chlorophenyl)-2-pyrazoline (23). Cream solid; mp 232.5–233.5 °C. IR cm^{-1} : 1763, 1683 (C=O), 1609, 1573, 1443 (C=C, C=N), 1395, 1243, 1207, 1026 (C–O–C, C–N). For 1H NMR, ^{13}C NMR, and mass data, see the [Supporting Information](#). Elemental analysis calculated (%) for $C_{26}H_{22}ClN_3O_4$: C 65.62, H 4.66, N 8.83. Found: C 65.46, H 4.60, N 8.88.

1-[2-(5-Methyl-2-benzoxazolinone-3-yl)acetyl]-3-(4-methoxyphenyl)-5-(2-chlorophenyl)-2-pyrazoline (24). White solid; mp 221–222 °C. IR cm^{-1} : 1771, 1664 (C=O), 1605, 1503, 1459 (C=C, C=N), 1392, 1255, 1172, 1014 (C–O–C, C–N). For 1H NMR, ^{13}C NMR, and mass data, see the [Supporting Information](#). Elemental analysis calculated (%) for $C_{26}H_{22}ClN_3O_4$: C 65.62, H 4.66, N 8.83. Found: C 65.75, H 4.57, N 8.87.

1-[2-(5-Chloro-2-benzoxazolinone-3-yl)acetyl]-3-phenyl-5-(4-methylphenyl)-2-pyrazoline (25). White solid; mp 174.5–175 °C. IR cm^{-1} : 2951, 2925 (C–H), 1782, 1679 (C=O), 1610, 1489, 1441 (C=C, C=N), 1383, 1353, 1305, 1240, 1146, 1115, 1061, 1025 (C–O–C, C–N). For 1H NMR, ^{13}C NMR, and mass data, see the [Supporting Information](#). Elemental analysis calculated (%) for $C_{25}H_{20}ClN_3O_3$: C 67.34, H 4.52, N 9.42. Found: C 67.15, H 4.72, N 9.59.

1-[2-(5-Chloro-2-benzoxazolinone-3-yl)acetyl]-3-phenyl-5-(3-methoxyphenyl)-2-pyrazoline (26).³⁵ Cream solid; mp 212–214 °C. IR cm^{-1} : 3071, 3027, 2948, 2917, 2826 (C–H), 1763, 1669 (C=O), 1486, 1442 (C=C, C=N), 1384, 1257, 1240, 1020 (C–O–C, C–N). For 1H NMR, ^{13}C NMR, and mass data, see the [Supporting Information](#). Elemental analysis calculated (%) for $C_{25}H_{20}ClN_3O_4$: C 65.01, H 4.36, N 9.10. Found: C 65.25, H 4.70, N 9.12.

1-[2-(5-Chloro-2-benzoxazolinone-3-yl)acetyl]-3-phenyl-5-(3,4-methoxyphenyl)-2-pyrazoline (27).³⁵ White solid; mp 197–199 °C. IR cm^{-1} : 3070, 3000, 2937, 2842 (C–H), 1765, 1672 (C=O), 1617, 1488, 1448 (C=C, C=N), 1389, 1235, 1148, 1029 (C–O–C, C–N). For 1H NMR, ^{13}C NMR, and mass data, see the [Supporting Information](#). Elemental analysis calculated (%) for $C_{26}H_{22}ClN_3O_5$: C 63.48, H 4.51, N 8.54. Found: C 63.10, H 4.44, N 8.70.

1-[2-(5-Chloro-2-benzoxazolinone-3-yl)acetyl]-3-(4-methylphenyl)-5-phenyl-2-pyrazoline (28). White solid; mp 174–176 °C. IR cm^{-1} : 3055, 2952 (C–H), 1775, 1676 (C=O), 1605, 1487, 1444 (C=C, C=N), 1385, 1318, 1243, 1014 (C–O–C, C–N). For 1H NMR, ^{13}C NMR, and mass data, see the [Supporting Information](#). Elemental analysis calculated (%) for $C_{25}H_{20}ClN_3O_3$: C 67.34, H 4.52, N 9.42. Found: C 67.17, H 4.73, N 9.60.

1-[2-(5-Chloro-2-benzoxazolinone-3-yl)acetyl]-3-(4-methylphenyl)-5-(2,3-dimethoxyphenyl)-2-pyrazoline (29).³⁵ White solid; mp 183–184 °C. IR cm^{-1} : 3019, 2960, 3944, 2838 (C–H), 1771, 1681 (C=O), 1613, 1484, 1442 (C=C, C=N), 1378, 1267, 1216, 1073, 1015 (C–O–C, C–N). For 1H NMR, ^{13}C NMR, and mass data, see the [Supporting Information](#). Elemental analysis calculated (%) for $C_{27}H_{24}ClN_3O_5$: C 64.10, H 4.78, N 8.31. Found: C 64.00, H 4.74, N 8.54.

1-[2-(5-Chloro-2-benzoxazolinone-3-yl)acetyl]-3-(4-methoxyphenyl)-5-phenyl-2-pyrazoline (30). Cream solid; mp 165–167 °C. IR cm^{-1} : 2944, 2842 (C–H), 1775, 1668 (C=O), 1601, 1487, 1455 (C=C, C=N), 1381, 1251, 1176, 1018 (C–O–C, C–N). For 1H NMR, ^{13}C NMR, and mass data, see the [Supporting Information](#). Elemental analysis calculated (%) for $C_{25}H_{20}ClN_3O_4$: C 65.01, H 4.36, N 9.10. Found: C 64.66, H 4.64, N 9.28.

1-[2-(5-Chloro-2-benzoxazolinone-3-yl)acetyl]-3-(4-methoxyphenyl)-5-(2,3-dimethoxyphenyl)-2-pyrazoline (31). Cream solid; mp 132–134 °C. IR cm^{-1} : 3014, 2951, 2831 (C–H), 1769, 1653

(C=O), 1613, 1520, 1490, 1463 (C=C, C=N), 1380, 1338, 1248, 1176, 1065, 1022, 1002 (C–O–C, C–N). For 1H NMR, ^{13}C NMR, and mass data, see the [Supporting Information](#). Elemental analysis calculated (%) for $C_{27}H_{24}ClN_3O_6 \cdot 0.9CHCl_3$: C 53.24, H 3.99, N 6.68. Found: C 53.10, H 3.78, N 6.93.

1-[2-(5-Chloro-2-benzoxazolinone-3-yl)acetyl]-3-(2-methoxyphenyl)-5-(2-chlorophenyl)-2-pyrazoline (32). White solid; mp 217.5–219 °C. IR cm^{-1} : 3074, 2944, 2830 (C–H), 1763, 1668 (C=O), 1593, 1491, 1436 (C=C, C=N), 1385, 1239, 1121, 1022 (C–O–C, C–N). For 1H NMR, ^{13}C NMR, and mass data, see the [Supporting Information](#). Elemental analysis calculated (%) for $C_{25}H_{19}Cl_2N_3O_4$: C 60.50, H 3.86, N 8.47. Found: C 60.48, H 3.93, N 8.74.

1-[2-(5-Chloro-2-benzoxazolinone-3-yl)acetyl]-3-(3-methoxyphenyl)-5-(2-chlorophenyl)-2-pyrazoline (33). White solid; mp 211–211.5 °C. IR cm^{-1} : 3070, 2948, 2834 (C–H), 1767, 1676 (C=O), 1597, 1491, 1440 (C=C, C=N), 1381, 1306, 1235, 1117, 1018 (C–O–C, C–N). For 1H NMR, ^{13}C NMR, and mass data, see the [Supporting Information](#). Elemental analysis calculated (%) for $C_{25}H_{19}Cl_2N_3O_4$: C 60.50, H 3.86, N 8.47. Found: C 60.21, H 3.70, N 8.53.

1-[2-(5-Chloro-2-benzoxazolinone-3-yl)acetyl]-3-(4-methoxyphenyl)-5-(2-chlorophenyl)-2-pyrazoline (34). Cream solid; mp 213–215 °C. IR cm^{-1} : 3067, 2941, 2838 (C–H), 1779, 1664 (C=O), 1605, 1491, 1459 (C=C, C=N), 1385, 1251, 1172, 1109, 1030, 1014 (C–O–C, C–N). For 1H NMR, ^{13}C NMR, and mass data, see the [Supporting Information](#). Elemental analysis calculated (%) for $C_{25}H_{19}Cl_2N_3O_4$: C 60.50, H 3.86, N 8.47. Found: C 60.55, H 4.04, N 8.68.

N'-(1,3-Diphenylallylidene)-2-(2-benzoxazolinone-3-yl)acetohydrazide (35). Yellow solid; mp 162–163 °C. IR cm^{-1} : 3201 (N–H), 3102, 3004, 2944 (C–H, aliphatic), 1756, 1678 (C=O), 1617, 1487, 1430 (C=C, C=N), 1372, 1229, 1097, 1022 (C–O–C, C–N). For 1H NMR, ^{13}C NMR, and mass data, see the [Supporting Information](#). Elemental analysis calculated (%) for $C_{24}H_{19}N_3O_3$: C 72.53, H 4.82, N 10.57. Found: C 72.39, H 4.73, N 10.57.

N'-[1-Phenyl-3-(3-methoxyphenyl)allylidene]-2-(2-benzoxazolinone-3-yl)acetohydrazide (36). Cream solid; mp 150–152 °C. IR cm^{-1} : 1781, 1687 (C=O), 1604, 1488, 1435 (C=C, C=N), 1386, 1238, 1020 (C–O–C, C–N). For 1H NMR, ^{13}C NMR, and mass data, see the [Supporting Information](#). Elemental analysis calculated (%) for $C_{25}H_{21}N_3O_4$: C 70.25, H 4.95, N 9.83. Found: C 70.00, H 4.84, N 9.80.

N'-[1-(2-Methoxyphenyl)-3-(2-chlorophenyl)allylidene]-2-(2-benzoxazolinone-3-yl)acetohydrazide (37). Yellow solid; mp 212–213 °C. IR cm^{-1} : 3208 (N–H), 3114, 3067, 3004, 2972, 2952, 2838 (C–H), 1768, 1687 (C=O), 1605, 1574, 1489, 1433 (C=C, C=N), 1364, 1241, 1107, 1085, 1020 (C–O–C, C–N). For 1H NMR, ^{13}C NMR, and mass data, see the [Supporting Information](#). Elemental analysis calculated (%) for $C_{25}H_{20}ClN_3O_4$: C 65.01, H 4.36, N 9.10. Found: C 65.12, H 4.22, N 9.26.

N'-[1-(4-Methoxyphenyl)-3-(2-chlorophenyl)allylidene]-2-(2-benzoxazolinone-3-yl)acetohydrazide (38). Yellow solid; mp 184.5–185.5 °C. IR cm^{-1} : 1783, 1683 (C=O), 1607, 1509, 1488 (C=C, C=N), 1365, 1252, 1174, 1102, 1021 (C–O–C, C–N). For 1H NMR, ^{13}C NMR, and mass data, see the [Supporting Information](#). Elemental analysis calculated (%) for $C_{25}H_{20}ClN_3O_4$: C 65.01, H 4.36, N 9.10. Found: C 65.14, H 4.45, N 9.23.

N'-[1-(2-Methoxyphenyl)-3-phenylallylidene]-2-(5-methyl-2-benzoxazolinone-3-yl)acetohydrazide (39). Yellow solid; mp 139–142 °C. IR cm^{-1} : 3192 (N–H), 2936, 2845 (C–H), 1775, 1668 (C=O), 1605, 1494, 1456 (C=C, C=N), 1381, 1305, 1241, 1175, 1129, 1023 (C–O–C, C–N). For 1H NMR, ^{13}C NMR, and mass data, see the [Supporting Information](#). Elemental analysis calculated (%) for $C_{26}H_{23}N_3O_4$: C 70.74, H 5.25, N 9.52. Found: C 70.67, H 5.05, N 9.69.

N'-[1-(2-Methoxyphenyl)-3-(2-chlorophenyl)allylidene]-2-(5-methyl-2-benzoxazolinone-3-yl)acetohydrazide (40). Yellow solid; mp 222–224 °C. IR cm^{-1} : 3212 (N–H), 2834 (C–H), 1768, 1688 (C=O), 1597, 1492, 1433 (C=C, C=N), 1388, 1241, 1085, 1021 (C–O–C, C–N). For 1H NMR, ^{13}C NMR, and mass data, see the

Supporting Information. Elemental analysis calculated (%) for $C_{26}H_{22}ClN_3O_4$: C 65.62, H 4.66, N 8.83. Found: C 65.53, H 4.86, N 9.03.

N'-[1-Phenyl-3-(2-methoxyphenyl)allylidene]-2-(5-chloro-2-benzoxazolinone-3-yl)acetohydrazide (**41**). Cream solid; mp 136–138 °C. IR cm^{-1} : 1782, 1666 (C=O), 1619, 1528, 1490 (C=C, C=N), 1384, 1241, 1108, 1018 (C–O–C, C–N). For 1H NMR, ^{13}C NMR, and mass data, see the [Supporting Information](#). Elemental analysis calculated (%) for $C_{25}H_{20}ClN_3O_4$: C 65.01, H 4.36, N 9.10. Found: C 65.37, H 4.43, N 9.30.

N'-[1-(4-Methoxyphenyl)-3-(2,3-dimethoxyphenyl)allylidene]-2-(5-chloro-2-benzoxazolinone-3-yl)acetohydrazide (**42**). White solid; mp 172–173.5 °C. IR cm^{-1} : 3328 (N–H), 3060, 2933, 2833 (C–H), 1788, 1686 (C=O), 1608, 1572, 1493, 1441 (C=C, C=N), 1382, 1338, 1249, 1172, 1066, 1016, 1003 (C–O–C, C–N). For 1H NMR, ^{13}C NMR, and mass data, see the [Supporting Information](#). Elemental analysis calculated (%) for $C_{27}H_{24}ClN_3O_6$: C 62.13, H 4.63, N 8.05. Found: C 62.08, H 4.69, N 8.25.

N'-[1-(2-Methoxyphenyl)-3-(2-chlorophenyl)allylidene]-2-(5-chloro-2-benzoxazolinone-3-yl)acetohydrazide (**43**). Yellow solid; mp 214–216 °C. IR cm^{-1} : 3204 (N–H), 3087, 3004, 2942, 2839 (C–H), 1781, 1686 (C=O), 1604, 1572, 1490, 1434 (C=C, C=N), 1384, 1252, 1110, 1084, 1019 (C–O–C, C–N). For 1H NMR, ^{13}C NMR, and mass data, see the [Supporting Information](#). Elemental analysis calculated (%) for $C_{25}H_{19}Cl_2N_3O_4$: C 60.50, H 3.86, N 8.47. Found: C 60.49, H 3.97, N 8.56.

X-ray Crystal Structure Determination. Data collection measurements for cream color single crystal of compound **10** and yellow color single crystal of compound **43** suitable for data collection were selected and performed at 293 K using an Agilent Xcalibur Eos diffractometer with CrysAlis PRO⁶¹ and graphite-monochromated Mo $K\alpha$ radiation ($\lambda = 0.71073 \text{ \AA}$). The structure was solved by direct methods by SHELXS-97⁶² within WINGX⁶³ suite of software. The refinement was carried out by full-matrix least-squares method on F^2 using SHELXL-97.⁶⁴ All H atoms were constrained to ride on their parent atoms, with C–H = 0.93–0.98 Å, N–H = 0.86 Å and $U_{iso}(H) = 1.2U_{eq}(C,N,O)$. The crystallographic data as well as details of the data collection and refinement results for the compounds are listed in [Table S5](#), [Supporting Information](#).⁶¹ Molecular diagrams were created using ORTEP-3.⁶⁵ Geometric calculations were performed using PLATON.⁶⁶

Molecular Modeling Studies. Enzyme Preparation. The crystal structure of hMAO-A, which is co-crystallized with harmine (a reversible inhibitor), and the crystal structure of hMAO-B, which is complexed with safinamide (a reversible inhibitor), were used for protein setup (<http://www.rcsb.org>), for MAO-A pdb code: 2Z5X; hMAO-A in complex with harmine, resolution 2.2 Å⁶⁷ and for MAO-B pdb code: 2VSZ; hMAO-B in complex with inhibitor safinamide, resolution 1.6 Å.⁶⁸ All water molecules, inhibitors, and noninteracting ions were cleared from each structure before being used in the docking studies. The initial oxidized form of the FAD was used in all docking studies. One of the two subunits was taken as the target structure for MAO-A and MAO-B. Each protein's geometry was first optimized by a fast Dreiding-like force field and then submitted to the “Clean Geometry” toolkit of Discovery Studio (Accelrys, Inc.) for a more complete check. Missing hydrogen atoms were added based on the protonation state of the titratable residues at a pH of 7.4. The ionic strength was set to 0.145, and the dielectric constant was set to 10.

Ligand Setup. The 3D structures of ligand molecules were built, optimized at the (PM3) level, and saved in pdb format. The AutoDock Tools (vv.1.5.4) (ADT) 69 graphical user interface program⁶⁹ was employed to generate grid parameter file (gpf) and docking parameter file (dpf) as docking input files.

Docking Calculations. Docking was carried out using AutoDock 4.2.6 program⁷⁰ using HPxw8600_Work_Station. The coordinates of the N5 atoms of the flavin cofactor were chosen as the grid centers for both MAO-A and MAO-B isozymes. The grid box sizes were adjusted to cover the entire binding site: X, Y, Z; 70, 70, 70 Å dimensions, respectively. Lamarckian genetic algorithm (LGA), which uses

semiempirical force field with an improved unbound state model as well as its updated desolvation term, to estimate the free energy of binding, was utilized for the search of optimal ligand binding conformation. The detailed docking procedures are given elsewhere.⁷¹ Accelrys Visualization 4.5 program was used for rendering the 2D and 3D pictures.

Biological Activity. MAO Activity Determination. The chemicals and recombinant hMAO enzymes were obtained from Sigma-Aldrich (Munich, Germany). A fluorimetric method, Amplex Red MAO assay kit (Molecular Probes), was performed following the instructions of the manufacturer. p-Tyramine (0.05–0.50 mM) was used as the common substrate for both hMAO-A and -B. Recombinant enzymes were diluted in reaction buffer (containing 0.25 M sodium phosphate, pH 7.4). Enzyme solution (100 μ L) was used for each reaction. H_2O_2 working solution (20 mM) was diluted to the final concentration of 10 μ M in reaction buffer and used as the positive control. The negative control was prepared as the reaction buffer without H_2O_2 . The diluted enzyme samples and controls (100 μ L) were pipetted into separate wells of a microplate. The reaction was started by adding 100 μ L of the Amplex Red working solution to each microplate well. The mixtures were incubated for 30 min at room temperature in the dark. Fluorescence was measured at multiple time points (excitation: 530 nm and emission: 590 nm). The obtained control values were subtracted to correct the background fluorescence. The possible fluorescence due to nonenzymatic inhibition was determined by adding the compounds to solutions containing only the Amplex Red reagent. HRP activity was not inhibited by newly synthesized compounds in the test medium.^{72,73} MAO activity was expressed as nmol/h/mg.

Kinetic Determination. Synthesized compounds with a maximum concentration of 1% were prepared in DMSO and used in a concentration range of 0.01 μ M to 10.00 mM. Selegiline was dissolved also in DMSO in the concentration range of 0.01–100.00 μ M. MAO inhibition was examined using Lineweaver–Burk plotting. K_i values were determined from the x -axis intercept as $-K_i$. Each K_i value is the representative of single determination, where the correlation coefficient (R^2) of the replot of the slopes versus the inhibitor concentrations was at least 0.98. SI was calculated as $K_i(\text{hMAO-A})/K_i(\text{hMAO-B})$. The protein was determined using Pierce Coomassie (Bradford) Protein Assay Kit (Cat no: 23200), which is based on the Bradford method.⁷⁴

Reversibility Assay. The dialysis method was performed as previously described for measuring the MAO inhibition.⁷⁵ Dialysis tubings with a molecular weight cutoff of 12 000 were used. Sample capacity was 0.5–10 mL. hMAO-A or hMAO-B enzymes (1 U/mL) and the inhibitors were incubated in potassium phosphate buffer (0.05 M, pH 7.4, 5% sucrose containing 1% DMSO) for 15 min at 37 °C. The inhibitor concentrations used were 4-fold of the IC_{50} values for the inhibition of hMAO-A and -B. Reaction mixtures having the same amount of hMAO-A and -B were also preincubated with the reference inhibitors. Enzyme–inhibitor mixtures were subsequently dialyzed at 4 °C in dialysis buffer (100 mM potassium phosphate, pH 7.4, 5% sucrose). The dialysis buffer was replaced with fresh buffer two times during 24 h of dialysis. After the dialysis, dialyzed and undialyzed mixtures were simultaneously assayed for MAO-A activity to evaluate the reversibility of the inhibition produced by the test compounds. All reactions were carried out in triplicate, and the residual enzyme activity was expressed as mean \pm SEM.

In Vitro Cytotoxicity Assay. Cell viability was measured by MTT assay using Human hepatoma cells HepG2 (Invitrogen).⁷⁶ The novel compounds (1, 5, and 25 μ M) or 0.1% DMSO as a vehicle control are used for the assay. Results were expressed as mean \pm SEM. Differences are considered statistically significant at $p < 0.05$.

In Vitro Blood–Brain Barrier Permeation Assay (PAMPA–BBB). The brain penetration ability of the compounds was determined using a PAMPA–BBB according to a previous method (Cyprotex).³⁷ Briefly, compounds and the reference drugs dissolved in DMSO were diluted with PBS/EtOH (70:30) to give a final concentration of 25 μ g/mL. The diluted solution (200 μ L) was added to the donor wells, and PBS/EtOH (300 μ L, 70:30) solution was

added to the acceptor wells. The donor filter plate was placed on the acceptor plate and kept at 25 °C for 16 h. The donor plate was removed, and the concentrations of the compounds in the wells were measured using a UV plate reader.

Pharmacological Tests. Animals. Albino male CD-1 mice (20–25 g) were used. The animals were kept in a room at a constant temperature under 12 h day/12 h night period with ad libitum access to food and water. All animal experiments were performed with the permission of Hacettepe University Animal Experimentations Local Ethics Board (2012/39, 2014/20).

Drug Administration. The compounds (30 mg/kg) and moclobemide (20 mg/kg) were administered orally with gavage in 200 μ L of 0.5% carboxymethylcellulose (CMC) solution. The control group was only administered with vehicle (0.5% CMC/200 μ L/each dose). All experiments were performed at the same time of the day, 1 h after the last administration of the drugs. Doses of 1, 3, 10, and 20 mg/kg/day for moclobemide and 1, 3, 10, and 30 mg/kg/day for compounds were administered during 7 days for the dose–response study.

Porsolt's Forced Swim Test (PFST). A modified Porsolt's forced swim test was used for the evaluation of antidepressant activity of synthesized compounds.^{77,78} Cylindrical glass tanks (19 cm height x 12 cm diameter) were used in the experiments. The cylinders were filled with water at 25 \pm 1 °C, and the water depth was adjusted to 15 cm. The mice were individually forced to swim. The duration of immobility or struggling with only small limb movements in a period of 6 min was scored. Scoring was performed every 60 s for 6 min. Immobility was judged when the mice remained floating in the water, whereas struggling was judged when the mice made active motions necessary to maintain its head above water. Immobility was regarded as depression-like behavior (behavioral despair).

Open-Field Test (OFT). Open-field test was used for assessing the changes of locomotor activity of the mice. The test was performed according to Painsipp, Wultsch et al. (2008)⁷⁹ and Brunner, Farzi et al. (2014).⁸⁰ The compounds and moclobemide were given subchronically as described above. Briefly, the mice were put in the center of a 50 \times 50 \times 30 cm³ black plastic box individually and tracked for 5 min with a video camera system (VideoMot2, TSE). The total distance traveled in the box was measured in 5 min. After the behavioral tests, the mice were sacrificed by cervical dislocation and their brain tissue was isolated for biochemical experiments.

Determination of Monoamine Levels in Brain Tissue. Determination of MAO Activity. Brain tissue was homogenized in 10 mM phosphate buffer pH 7.4 containing 0.25 M sucrose, following differential centrifugation to obtain the mitochondrial fraction.⁸¹ Tissue protein content was determined using the Bradford method.⁷⁴ Tissue MAO-A and B activities were determined using monoamine oxidase assay kit (Sigma-Aldrich, MAK 136) according to the manufacturer's instructions. The MAO activity was expressed as nmol/min/mg.

Determination of Serotonin (5-HT) Level. The brain tissue 5-HT content was determined after homogenization in phosphate buffer (pH 7.4) using Mouse 5-HT Elisa kit based on the competitive enzyme-linked immunosorbent assay (ELISA) using a monoclonal anti-5-HT antibody and a 5-HT-HRP conjugate. Catalog Number: MBS723181 (MyBioSource) The 5-HT concentration in each sample is interpolated from a prepared standard curve and expressed as μ g/g tissue.

Determination of Dopamine Level. Dopamine concentration in brain tissue was determined after tissue homogenization in PBS using Mouse Dopamine ELISA Kit (Cat. no: MBS035672) (MyBioSource) according to the manufacturer's manual. A standard curve was prepared using the professional curve fitting software, and results were expressed as μ g/g tissue.

Determination of Transmitter Metabolite Levels. DOPAC and 5-HIAA were measured according to a previous method based on electrochemical detection by Nucleosil 5 C18 (Dionex) column.⁸² The mobile phase consisted of a 0.1 M citrate/acetate buffer pH 3.9 with 10% methanol, 1 M ethylenediamine tetraacetic acid (EDTA), and 1.2 heptane sulfonic acid. The detector voltage conditions were

D1 (+0.05), D2 (–0.39), and the guard cell (+0.40). Results were expressed as μ g/g tissue.

Statistical Analysis. Statistical analysis of biochemical tests was conducted using GraphPad Prism 4.03 (GraphPad Software, San Diego, CA, ABD) compatible with Windows. Student's *t* test was used to achieve comparison between study groups. Results were expressed as mean \pm SD, and *p* < 0.05 was accepted statistically significant. Data for pharmacological tests were analyzed by one-way analysis of variance (ANOVA) followed by *post hoc* Dunnett's test. Data were expressed as mean \pm SEM. *p* < 0.05 was accepted statistically significant.

■ ASSOCIATED CONTENT

Supporting Information

The Supporting Information is available free of charge at <https://pubs.acs.org/doi/10.1021/acs.jmedchem.0c01504>.

Spectral data of the newly synthesized compounds; X-ray crystal structure; druglikeness and ADMET predictions; and additional molecular modeling data of selected compounds (PDF)

Molecular formula strings for the newly synthesized compounds (CSV)

■ AUTHOR INFORMATION

Corresponding Authors

Gulberk Ucar – Department of Biochemistry, Faculty of Pharmacy, Hacettepe University, 06100 Ankara, Turkey; Email: gulberk.ucar@gmail.com

Nesrin Gokhan-Kelekci – Department of Pharmaceutical Chemistry, Faculty of Pharmacy, Hacettepe University, 06100 Ankara, Turkey; orcid.org/0000-0001-7383-8443; Email: onesrin@gmail.com

Authors

Umut Salgin-Goksen – Department of Pharmaceutical Chemistry, Faculty of Pharmacy, Hacettepe University, 06100 Ankara, Turkey; Turkish Medicines and Medical Devices Agency, Analyses and Control Laboratories, 06100 Ankara, Turkey

Gokcen Telli – Department of Pharmacology, Faculty of Pharmacy, Hacettepe University, 06100 Ankara, Turkey

Acelya Erikci – Department of Biochemistry, Faculty of Pharmacy, Lokman Hekim University, 06510 Ankara, Turkey

Ezgi Dedecengiz – Department of Physics Engineering, Faculty of Engineering, Hacettepe University, 06800 Ankara, Turkey

Banu Cahide Tel – Department of Pharmacology, Faculty of Pharmacy, Hacettepe University, 06100 Ankara, Turkey

F. Betul Kaynak – Department of Physics Engineering, Faculty of Engineering, Hacettepe University, 06800 Ankara, Turkey

Kemal Yelekci – Department of Bioinformatics and Genetics, Faculty of Engineering and Natural Sciences, Kadir Has University, 34083 Fatih, Istanbul, Turkey; orcid.org/0000-0002-0052-4926

Complete contact information is available at: <https://pubs.acs.org/doi/10.1021/acs.jmedchem.0c01504>

Author Contributions

N.G.K. designed the study; U.S.G. and N.G.K. synthesized the new compounds and evaluated their structures; E.D. and F.B.K. provided the X-ray crystal structure of the compounds; A.E. and G.U. carried out and evaluated the *in vitro* and *ex vivo*

biochemical tests; G.T. and B.C.T. accomplished the pharmacological part; K.Y. performed the computational studies; G.T. and A.E. conducted the statistical analyses; N.G.K., G.U., and B.C.T. interpreted the data; N.G.K. and G.U. edited the manuscript and provided critical revisions; and N.G.K. is the guarantor.

Notes

The authors declare no competing financial interest.

ACS includes X-ray crystallographic data for compounds **10** and **43**; druglikeness and ADMET properties, docking results of compounds **14S**, **21R**, and **42**; ^1H NMR, ^{13}C NMR, and mass interpretations; and all spectral data and molecular formula strings of the synthesized compounds. Crystallographic data for the structures reported in this paper have been deposited with the Cambridge Crystallographic Data Centre (The Director, CCDC, 12 Union Road, Cambridge, CB2 1EZ, U.K.; E-mail: deposit@ccdc.cam.ac.uk; www: <http://www.ccdc.cam.ac.uk>; fax: +44 1223 336033) and are available free of charge on request, quoting the Deposition No. CCDC 1411742 for (**10**) and 1411743 for (**43**).

ACKNOWLEDGMENTS

This study was supported by grants from The Scientific and Technological Research Council of Turkey (TUBITAK) (112T746) and the Hacettepe University Scientific Research Projects Coordination Unit (012D06301001 and 1527). The authors are thankful to Prof. Dr. Erhan Palaska for providing MS spectra. They thank Hacettepe University Technology Transfer Center for providing funding and English-language editing service.

ABBREVIATIONS USED

PFST, Porsolt's forced swim test; MAOIs, monoamine oxidase inhibitors; SSRI, selective serotonin reuptake inhibitors; TCA, tricyclic antidepressants; CNS, central nervous system; BBB, blood-brain barrier; PAMPA, parallel artificial membrane permeation assay; OFT, open-field test; 5-HIAA, 5-hydroxyindoleacetic acid; DOPAC, 3,4-dihydroxyphenylacetic acid; RIMAs, selective reversible inhibitors of MAO-A; MTT, 3-[4,5-dimethylthiazol-2-yl]-2,5-diphenyl-tetrazolium bromide; DMEM, Dulbecco's modified Eagle's medium; FBS, fetal bovine serum; DMSO, dimethylsulfoxide; PBL, polar brain lipid; CMC, carboxymethylcellulose

REFERENCES

- (1) World Federation for Mental Health, 2012. DEPRESSION: A Global Crisis. https://www.who.int/mental_health/management/depression/wfmh_paper_depression_wmhd_2012.pdf?Ua=1 (accessed Jun 25, 2020).
- (2) Murray, C. J.; Lopez, A. D. Alternative Projections of Mortality and Disability by Cause 1990-2020: Global Burden of Disease Study. *Lancet* **1997**, *349*, 1498–1504.
- (3) Musselman, D. L.; Evans, D. L.; Nemeroff, C. B. The relationship of depression to cardiovascular disease: epidemiology, biology, and treatment. *Arch. Gen. Psychiatry* **1998**, *55*, 580–592.
- (4) Michelson, D.; Stratakis, C.; Hill, L.; Reynolds, J.; Galliven, E.; Chrousos, G.; Gold, P. Bone Mineral Density in Women with Depression. *N. Engl. J. Med.* **1996**, *335*, 1176–1181.
- (5) Schulz, R.; Beach, S. R.; Ives, D. G.; Martire, L. M.; Ariyo, A. A.; Kop, W. J. Association Between Depression and Mortality in Older Adults: the Cardiovascular Health Study. *Arch. Intern. Med.* **2000**, *160*, 1761–1768.

- (6) Seney, M. L.; Sibille, E. Sex Differences in Mood Disorders: Perspectives from Humans and Rodent Models. *Biol. Sex Differ.* **2014**, *5*, No. 17.
- (7) Collins, G. G.; Sandler, M.; Williams, E. D.; Youdim, M. B. Multiple Forms Of Human Brain Mitochondrial Monoamine Oxidase. *Nature* **1970**, *225*, 817–820.
- (8) Johnston, J. P. Some Observations Upon A New Inhibitor Of Monoamine Oxidase In Brain Tissue. *Biochem. Pharmacol.* **1968**, *17*, 1285–1297.
- (9) Knoll, J.; Magyar, K. Some Puzzling Pharmacological Effects Of Monoamine Oxidase Inhibitors. *Adv. Biochem. Psychopharmacol.* **1972**, *5*, 393–408.
- (10) O'Carroll, A. M.; Fowler, C. J.; Phillips, J. P.; Tobbia, I.; Tipton, K. F. The Deamination Of Dopamine By Human Brain Monoamine Oxidase. Specificity For The Two Enzyme Forms In Seven Brain Regions. *Naunyn-Schmiedeberg's Arch. Pharmacol.* **1983**, *322*, 198–202.
- (11) Wouters, J. Structural Aspects Of Monoamine Oxidase And Its Reversible Inhibition. *Curr. Med. Chem.* **1998**, *5*, 137–162.
- (12) Carreiras, C.; Marco, J. L. Recent Approaches To Novel Anti-Alzheimer Therapy. *Curr. Pharm. Des.* **2004**, *10*, 3167–3175.
- (13) Finberg, J. P. M. Update On The Pharmacology Of Selective Inhibitors Of Mao-A And Mao-B: Focus On Modulation Of Cns Monoamine Neurotransmitter Release. *Pharmacol. Ther.* **2014**, *143*, 133–152.
- (14) Yanez, M.; Padin, J. F.; Arranz-Tagarro, J. A.; Camina, M.; Laguna. History And Therapeutic Use Of MAO-A Inhibitors: A Historical Perspective Of MAO-A Inhibitors As Antidepressant Drug. *Curr. Med. Chem.* **2012**, *12*, 2275–2282.
- (15) Chimenti, F.; Maccioni, E.; Secci, D.; Bolasco, A.; Chimenti, P.; Granese, A.; Befani, O.; Turini, P.; Alcaro, S.; Ortuso, F.; Cirilli, R.; La Torre, F.; Cardia, M. C.; Distinto, S. Synthesis, Molecular Modeling Studies, And Selective Inhibitory Activity Against Monoamine Oxidase Of 1-Thiocarbamoyl-3,5-Diaryl-4,5-Dihydro-(1H)-Pyrazole Derivatives. *J. Med. Chem.* **2005**, *48*, 7113–7122.
- (16) Manna, F.; Chimenti, F.; Bolasco, A.; Secci, D.; Bizzarri, B.; Befani, O.; Turini, P.; Mondovi, B.; Alcaro, S.; Tafi, A. Inhibition Of Amine Oxidases Activity By 1-Acetyl-3,5-Diphenyl-4,5-Dihydro-(1H)-Pyrazole Derivatives. *Bioorg. Med. Chem. Lett.* **2002**, *12*, 3629–3633.
- (17) Secci, D.; Bolasco, A.; Chimenti, P.; Carradori, S. The State Of The Art Of Pyrazole Derivatives As Monoamine Oxidase Inhibitors And Antidepressant/Anticonvulsant Agents. *Curr. Med. Chem.* **2011**, *18*, 5114–5144.
- (18) Mathew, B.; Suresh, J.; Anbazhagan, S. Synthesis, Preclinical Evaluation And Antidepressant Activity Of 5-Substituted Phenyl-3-(Thiophen-2-Yl)-4, 5-Dihydro-1H-Pyrazole-1-Carbothioamides. *EXCLI J.* **2014**, *13*, 437–445.
- (19) Chimenti, F.; Bolasco, A.; Manna, F.; Secci, D.; Chimenti, P.; Befani, O.; Turini, P.; Giovannini, V.; Mondovi, B.; Cirilli, R.; La Torre, F. Synthesis And Selective Inhibitory Activity Of 1-Acetyl-3,5-Diphenyl-4,5-Dihydro-(1H)-Pyrazole Derivatives Against Monoamine Oxidase. *J. Med. Chem.* **2004**, *47*, 2071–2074.
- (20) Chimenti, F.; Fioravanti, R.; Bolasco, A.; Manna, F.; Chimenti, P.; Secci, D.; Rossi, F.; Turini, P.; Ortuso, F.; Alcaro, S.; Cardia, M. C. Synthesis, Molecular Modeling Studies And Selective Inhibitory Activity Against MAO Of N1-Propanoyl-3,5-Diphenyl-4,5-Dihydro-(1H)-Pyrazole Derivatives. *Eur. J. Med. Chem.* **2008**, *43*, 2262–2267.
- (21) Chimenti, F.; Carradori, S.; Secci, D.; Bolasco, A.; Bizzarri, B.; Chimenti, P.; Granese, A.; Yáñez, M.; Orallo, F. Synthesis And Inhibitory Activity Against Human Monoamine Oxidase Of N1-Thiocarbamoyl-3,5-Di(Hetero)Aryl-4,5-Dihydro-(1H)-Pyrazole Derivatives. *Eur. J. Med. Chem.* **2010**, *45*, 800–804.
- (22) Lamanna, C.; Sinicropi, M. S.; Pietrangeli, P.; Corbo, F.; Franchini, C.; Mondovi, B.; Scilimati, A. Synthesis And Biological Evaluation Of 3-Alkyloxazolidin-2-Ones As Reversible MAO Inhibitors. *Arkivoc* **2004**, *2004*, 118–130.
- (23) Mai, A.; Artico, M.; Esposito, M.; Sbardella, G.; Massa, S.; Befani, O.; Turini, P.; Giovannini, V.; Mondovi, B. 3-(1H-pyrrol-1-

yl)-2-oxazolidinones as Reversible, Highly Potent, And Selective Inhibitors Of Monoamine Oxidase Type A. *J. Med. Chem.* **2002**, *45*, 1180–1183.

(24) Close, W. J.; Tiffany, B. D.; Spielman, M. A. The Analgesic Activity of Some Benzoxazolone Derivatives. *J. Am. Chem. Soc.* **1949**, *71*, 1265–1268.

(25) Milcent, R.; Akhnazarian, A.; Lensen, N. Synthesis of 1-(2-hydroxyphenyl)-2,4-Imidazolidinedione Derivatives Through Cyclic Transformations Of Ethyl 2-Oxo-3(2H)-Benzoxazoleacetate Derivatives. *J. Heterocycl. Chem.* **1996**, *33*, 1829–1833.

(26) Çakir, B.; Yildirim, E.; Ercanli, T.; Erol, K.; Sahin, M. F. Synthesis And Anticonvulsant Activity Of Some (2/4-Substituted)-Benzaldehyde (2-Oxobenzothiazolin-3-Yl)Acetohydrazones. *II Farmaco* **1999**, *54*, 842–845.

(27) Gökçe, M.; Geciken, A. E.; Yildirim, E.; Tosuni, A. U. Synthesis And Anticonvulsant Activity Of 5-Chloro-2(3H)-Benzoxazolinone-3-Acetyl-2-(O/P-Substituted Benzal) Hydrazone Derivatives. *Arzneimittelforschung* **2008**, *58*, 537–542.

(28) Salgin-Gökşen, U.; Gokhan-Kelekci, N.; Goktas, O.; Koysal, Y.; Kilic, E.; Isik, S.; Aktay, G.; Ozalp, M. 1-Acylthiosemicarbazides, 1,2,4-triazole-5(4H)-thiones, 1,3,4-thiadiazoles and hydrazones containing 5-methyl-2-benzoxazolinones: Synthesis, Analgesic-Anti-Inflammatory And Antimicrobial Activities. *Bioorg. Med. Chem.* **2007**, *15*, 5738–5751.

(29) Davey, W.; Tivey, D. J. Chalcones and Related Compounds. 4. Addition of Hydrogen Cyanide to Chalcones. *J. Chem. Soc.* **1958**, 1230–1236.

(30) Goksen, U. S.; Sarigul, S.; Bultinck, P.; Herrebout, W.; Dogan, I.; Yelekci, K.; Ucar, G.; Gokhan Kelekci, N. Absolute Configuration And Biological Profile Of Pyrazoline Enantiomers As MAO Inhibitory Activity. *Chirality* **2019**, *31*, 21–33.

(31) Yang, H.; Lou, C.; Sun, L.; Li, J.; Cai, Y.; Wang, Z.; Li, W.; Liu, G.; Tang, Y. Admetsar 2.0: Web-Service For Prediction And Optimization Of Chemical ADMET Properties. *Bioinformatics* **2019**, *35*, 1067–1069.

(32) Lipinski, C. A. Lead- And Drug-Like Compounds: The Rule-Of-Five Revolution. *Drug Discovery Today: Technol.* **2004**, *1*, 337–341.

(33) Di, L.; Kerns, E. H. *Drug-Like Properties: Concepts, Structure Design and Methods From ADME to Toxicity Optimization*, 2nd ed.; Academic Press: Massachusetts, 2016.

(34) Şahin, Z. S.; Salgin-Gökşen, U.; Gökhan Kelekçi, N.; Işık, Ş. Synthesis, Crystal Structures And DFT Studies Of 1-[2-(5-Methyl-2-Benzoxazolinone-3-Yl) Acetyl]-3-Phenyl-5-(3,4-Dimethoxyphenyl)-4,5-Dihydro-1H-Pyrazole And 1-[2-(5-Chloro-2-Benzoxazolinone-3-Yl)Acetyl]-3-Phenyl-5-(4-Methoxyphenyl)-4,5-Dihydro-1H-Pyrazole. *J. Mol. Struct.* **2011**, *1006*, 147–158.

(35) Gökşen, U. S.; Alpaslan, Y. B.; Kelekci, N.; Isik, S.; Ekizoglu, M. Synthesis, Crystal Structures And Theoretical Calculations Of New 1-[2-(5-Chloro-2-Benzoxazolinone-3-Yl)Acetyl]-3,5-Diphenyl-4,5-Dihydro-(1H)-Pyrazoles. *J. Mol. Struct.* **2013**, *1039*, 71–83.

(36) Carpenter, T. S.; Kirshner, D. A.; Lau, E. Y.; Wong, S. E.; Nilmeier, J. P.; Lightstone, F. C.; et al. A Method to Predict Blood-Brain Barrier Permeability of Drug-Like Compounds Using Molecular Dynamics Simulations. *Biophys. J.* **2014**, *107*, 630–641.

(37) Di, L.; Kerns, E. H.; Fan, K.; McConnell, O. J.; Carter, G. T. High Throughput Artificial Membrane Permeability Assay For Blood-Brain Barrier. *Eur J. Med. Chem.* **2003**, *38*, 223–232.

(38) Borsini, F.; Meli, A. Is The Forced Swimming Test A Suitable Model For Revealing Antidepressant Activity? *Psychopharmacology* **1988**, *94*, 147–160.

(39) Vaidya, A.; Pradhan, A.; Joshi, S. K.; Gopalakrishnan, S.; Dudani, I. Acquaintance With The Actuality: Community Diagnosis Programme Of Kathmandu Medical College At Gundu Village, Bhaktapur, Nepal. *Kathmandu Univ. Med. J.* **2008**, *6*, 128–134.

(40) Krishnan, V.; Nestler, E. J. Animal Models Of Depression: Molecular Perspectives. In *Molecular and functional models in neuropsychiatry*; Current Topics in Behavioral Neurosciences; Springer: Berlin, Heidelberg, 2011; Vol. 7, pp 121–147.

(41) Petit-Demouliere, B.; Chenu, F.; Bourin, M. Forced Swimming Test In Mice: A Review Of Antidepressant Activity. *Psychopharmacology* **2005**, *177*, 245–255.

(42) Yan, H. C.; Cao, X.; Das, M.; Zhu, X. H.; Gao, T. M. Behavioral Animal Models Of Depression. *Neurosci Bull* **2010**, *26*, 327–337.

(43) Castagné, V.; Moser, P.; Roux, S.; Porsolt, R. D. Rodent Models Of Depression: Forced Swim And Tail Suspension Behavioral Despair Tests In Rats And Mice. *Curr. Protoc. Neurosci.* **2011**, *55*, 8–10.

(44) Xu, Y.; Li, S.; Chen, R.; Li, G.; Barish, P. A.; You, W.; Chen, L.; Lin, M.; Ku, B.; Pan, J.; Ogle, W. O. Antidepressant-Like Effect Of Low Molecular Proanthocyanidin In Mice: Involvement Of Monoaminergic System. *Pharmacol., Biochem. Behav.* **2010**, *94*, 447–453.

(45) Drigues, N.; Poltyrev, T.; Bejar, C.; Weinstock, M.; Youdim, M. B. cDna Gene Expression Profile Of Rat Hippocampus After Chronic Treatment With Antidepressant Drugs. *J. Neural Transm.* **2003**, *110*, 1413–1436.

(46) Pare, C. M. The Present Status Of Monoamine Oxidase Inhibitors. *Br. J. Psychiatry* **1985**, *146*, 576–584.

(47) Baker, G. B.; Coutts, R. T.; McKenna, K. F.; Sherry-McKenna, R. Insights Into The Mechanisms Of Action Of The MAO Inhibitors Phenelzine And Tranylcypromine: A Review. *J. Psychiatr. Neurosci.* **1992**, *17*, 206–214.

(48) Stassen, H.; Angst, J.; Delini-Stula, A. Onset of improvement under fluoxetine and moclobemide. *Eur. Psychiatr.* **1998**, *13*, 128–133.

(49) Barbelivien, A.; Nyman, L.; Haapalinna, A.; Sirvio, J. Inhibition Of MAO-A Activity Enhances Behavioural Activity Of Rats Assessed Using Water Maze And Open Arena Tasks. *Pharmacol. Toxicol.* **2001**, *88*, 304–312.

(50) Cao, Y. Q.; Dai, Z.; Zhang, R.; Chen, B. H. Aldol Condensations Catalyzed By PEG400 And Anhydrous K₂CO₃ Without Solvent. *Synth. Commun.* **2005**, *35*, 1045–1049.

(51) Sarbhai, K. P.; Mathur, K. B. L. Some Arylation Reactions with Diazotized 3,4,5-Trimethoxyaniline - Preparation of 3,4,5-Trimethoxychalcone and 3,4,5-Trimethoxybenzaldehyde. *Indian J. Chem.* **1963**, *1*, 482.

(52) Koo, J. Syntheses in the Indene Series. *J. Am. Chem. Soc.* **1953**, *75*, 2000–2001.

(53) Wattanasin, S.; Murphy, W. S. An Improved Procedure for the Preparation of Chalcones and Related Enones. *Synthesis* **1980**, 647–650.

(54) Jaramillo, M. C.; Mora, C.; Vélez, L. E.; Arango, G. J.; Quijano, J. Biological evaluation of aromatic compounds as β -lactamase inhibitors. *Pharmacologyonline* **2006**, *3*, 650–655.

(55) Jaramillo, M. C.; Mora, C.; Velez, L. E.; Quijano, J. Kinetic and Theoretical Study of the Chalcones as Inhibitors of beta-Lactamase Enzyme. *Med. Chem.* **2009**, *5*, 434–439.

(56) Manolov, I.; Danchev, N. D. Synthesis And Pharmacological Investigations Of Some 4-Hydroxycoumarin Derivatives. *Archiv Der Pharmazie* **2003**, *336*, 83–94.

(57) Hanson, G. A. Synthesis Of Substituted 2-Hydroxyisophthalic Acids. *Bull. Soc. Chim. Belg.* **1956**, *65*, 700–705.

(58) Liu, X.; Go, M. L. Antiproliferative Properties Of Piperidinylochalcones. *Bioorg. Med. Chem.* **2006**, *14*, 153–163.

(59) Biradar, D. B.; Gau, H. M. Highly Enantioselective Conjugate Addition Of Diethylzinc To Substituted Chalcones Catalyzed By Cu(II) Complexes Of A Tridentate P,N,O Ligand. *Tetrahedron: Asymmetry* **2008**, *19*, 733–738.

(60) Wu, J.; Li, J.; Cai, Y.; Pan, Y.; Ye, F.; Zhang, Y.; Zhao, Y.; Yang, S.; Li, X.; Liang, G. Evaluation And Discovery Of Novel Synthetic Chalcone Derivatives As Anti-Inflammatory Agents. *J. Med. Chem.* **2011**, *54*, 8110–8123.

(61) Agilent, (2012). *CrysAlis PRO*; Agilent Technologies, Y.: Oxfordshire, England.

(62) Sheldrick, G. M. (1997). *SHELXS97. Program For The Solution Of Crystal Structures*; University of Göttingen: Germany.

- (63) Farrugia, L. J. WinGX. Suite For Small-Molecule Single-Crystal Crystallography. *J. Appl. Crystallogr.* **1999**, *32*, 837–838.
- (64) Sheldrick, G. M. (1997). *SHELXL97 Program For The Refinement Of Crystal Structures*. University of Göttingen: Germany.
- (65) Farrugia, L. J. ORTEP-3 for Windows-A Version of It ORTEP-III with a Graphical User Interface (GUI). *J. Appl. Crystallogr.* **1997**, *30*, 565.
- (66) Spek, A. L. PLATON. An Integrated Tool For The Analysis Of The Results Of A Single Crystal Structure Determination. *Acta Crystallogr., Sect. A: Found. Crystallogr.* **1990**, *A46*, c34.
- (67) Son, S. Y.; Ma, J.; Kondou, Y.; Yoshimura, M.; Yamashita, E.; Tsukihara, T. Structure Of Human Monoamine Oxidase A At 2.2-Å Resolution: The Control Of Opening The Entry For Substrates/Inhibitors. *Proc. Natl. Acad. Sci. U.S.A.* **2008**, *105*, 5739–5744.
- (68) Binda, C.; Wang, J.; Pisani, L.; Caccia, C.; Carotti, A.; Salvati, P.; Edmondson, D. E.; Mattevi, A. Structures Of Human Monoamine Oxidase B Complexes With Selective Noncovalent Inhibitors: Safinamide And Coumarin Analogs. *J. Med. Chem.* **2007**, *50*, 5848–5852.
- (69) Morris, G. M.; Huey, R.; Lindstrom, W.; Sanner, M. F.; Belew, R. K.; Goodsell, D. S.; Olson, A. AutoDock4 and AutoDockTools4: Automated Docking With Selective Receptor Flexibility. *J. Comput. Chem.* **2009**, *30*, 2785–2791.
- (70) Morris, G. M.; Goodsell, D. S.; Halliday, R. S.; Huey, R.; Hart, W. E.; Belew, R. K.; Olson, A. J. Automated Docking Using A Lamarckian Genetic Algorithm And Empirical Binding Free Energy Function. *J. Comput. Chem.* **1998**, *19*, 1639–1662.
- (71) Akdoğan, E. D.; Erman, B.; Yeleği, K. In Silico Design Of Novel And Highly Selective Lysine-Specific Histone Demethylase Inhibitors. *Turk J. Chem.* **2011**, *35*, 523–542.
- (72) Yáñez, M.; Fraiz, N.; Cano, E.; Orallo, F. Inhibitory Effects Of Cis- And Trans-Resveratrol On Noradrenaline And 5-Hydroxytryptamine Uptake And On Monoamine Oxidase Activity. *Biochem. Biophys. Res. Commun.* **2006**, *344*, 688–695.
- (73) Chimenti, F.; Maccioni, E.; Bolasco, A.; Manna, F.; Chimenti, P.; Secci, D.; Rossi, F.; Turini, P.; Ortuso, F.; Alcaro, S.; Cardia, M. C.; et al. Synthesis, Stereochemical Identification, And Selective Inhibitory Activity Against Human Monoamine Oxidase-B Of 2-Methylcyclohexylidene-(4-Arylthiazol-2-Yl)Hydrazones. *J. Med. Chem.* **2008**, *51*, 4874–4880.
- (74) Bradford, M. M. A Rapid And Sensitive Method For The Quantitation Of Microgram Quantities Of Protein Utilizing The Principle Of Protein-Dye Binding. *Anal. Biochem.* **1976**, *72*, 248–254.
- (75) Petzer, A.; Pienaar, A.; Petzer, J. P. The Inhibition Of Monoamine Oxidase By Esomeprazole. *Drug Res.* **2013**, *63*, 462–467.
- (76) Hansen, M. B.; Nielsen, S. E.; Berg, K. Re-Examination And Further Development Of A Precise And Rapid Dye Method For Measuring Cell Growth/Cell Kill. *J. Immunol. Methods* **1989**, *119*, 203–210.
- (77) Porsolt, R. D.; Anton, G.; Blavet, N.; Jalfre, M. Behavioural Despair In Rats: A New Model Sensitive To Antidepressant Treatments. *Eur. J. Pharmacol.* **1978**, *47*, 379–391.
- (78) Sherman, A. D.; Hegwood, T. S.; Baruah, S.; Waziri, R. Presynaptic Modulation Of Amino Acid Release From Synaptosomes. *Neurochem Res.* **1992**, *17*, 125–128.
- (79) Painsipp, E.; Wultsch, T.; Edelsbrunner, M. E.; Tasan, R. O.; Singewald, N.; Herzog, H.; Holzer, P. Reduced Anxiety-Like And Depression-Related Behavior In Neuropeptide Y Y4 Receptor Knockout Mice. *Genes, Brain Behav.* **2008**, *7*, 532–542.
- (80) Brunner, S. M.; Farzi, A.; Locker, F.; Holub, B. S.; Drexel, M.; Reichmann, F.; Lang, A. A.; Mayr, J. A.; Vilches, J. J.; Navarro, X.; Lang, R.; Sperk, G.; Holzer, P.; Kofler, B. GAL3 Receptor KO Mice Exhibit An Anxiety-Like Phenotype. *Proc. Natl. Acad. Sci. U.S.A.* **2014**, *111*, 7138–7143.
- (81) Sandri, G.; Panfilì, E.; Ernster, L. Hydrogen Peroxide Production By Monoamine Oxidase In Isolated Rat-Brain Mitochondria: Its Effect On Glutathione Levels And Ca²⁺ Efflux. *Biochim. Biophys. Acta, Gen. Subj.* **1990**, *1035*, 300–305.
- (82) Mena, M. A.; Garcia de Yebenes, M. J.; Taberero, C.; Casarejos, M. J.; Pardo, B.; Garcia de Yebenes, J. Effects Of Calcium Antagonists On The Dopamine System. *Clin. Neuropharmacol.* **1995**, *18*, 410–426.